

Ground-state energy of pionic hydrogen to one loop

J. Gasser¹, M.A. Ivanov², E. Lipartia^{3,4,5}, M. Mojžiš^{6,7}, and A. Rusetsky^{1,5}

- ¹ *Institute for Theoretical Physics, University of Bern, Sidlerstrasse 5, 3012 Bern, Switzerland*
² *Bogoliubov Laboratory of Theoretical Physics, Joint Institute for Nuclear Research, 141980 Dubna, Russia*
³ *Department of Theoretical Physics 2, Lund University, Solvegatan 14A, S22362 Lund, Sweden*
⁴ *Laboratory of Information Technologies, Joint Institute for Nuclear Research, 141980 Dubna, Russia*
⁵ *High Energy Physics Institute, Tbilisi State University, University St. 9, 380086 Tbilisi, Georgia*
⁶ *Department of Physics, University of Massachusetts, Amherst, MA 01003, USA*
⁷ *Department of Theoretical Physics, Comenius University, SK-28415 Bratislava, Slovakia*

the date of receipt and acceptance should be inserted later

Abstract. We investigate the ground-state energy of the π^-p atom (pionic hydrogen) in the framework of QCD+QED. In particular, we evaluate the strong energy-level shift. We perform the calculation at next-to-leading order in the low-energy expansion in the framework of the relevant effective field theory. The result provides a relation between the strong energy shift and the pion-nucleon S -wave scattering lengths - evaluated in pure QCD - at next-to-leading order in isospin breaking and in the low-energy expansion. We compare our result with available model calculations.

PACS. 11.30.Rd – 12.39.Fe – 13.40.Ks – 13.75.Gx – 36.10.Gv

Contents

1	Introduction	1
2	Threshold amplitude and the strong energy-level shift	3
3	Lagrangians	4
4	Tree contributions	6
5	Two-point functions of pion fields	6
6	Two-point function of baryon fields	8
7	Evaluation of S -matrix elements	10
8	The triangle diagram	10
9	The threshold amplitude at order p^3	11
10	The size of the low-energy constants	12
11	Ground-state energy-level shift	13
12	Summary and conclusions	15
A	Meson-meson and meson-nucleon Lagrangians	16
B	Divergent counterterms	17
C	Integrals	20
D	Contributions from individual Feynman diagrams	21
E	Figures	23

1 Introduction

The theory of strong interactions has entered a high precision phase in recent years, both experimentally and theoretically. On the experimental side, we mention i) the muon anomalous magnetic moment measurement at Brookhaven [1]. A calculation of $(g-2)_\mu$ that matches the foreseen experimental accuracy requires that the cross section $e^+e^- \rightarrow \pi^+\pi^-$ in the low-energy region is known to

better than one percent; ii) experiments that aim to determine hadronic scattering lengths with high precision are presently running at CERN [2] and at PSI [3,4]. On the theory side, the $\pi\pi$ scattering lengths have recently been calculated at the few-percent level in Ref. [5]. In this article, we are concerned with the ongoing experiment on the measurement of the energy levels and decays of the π^-p atom (pionic hydrogen) at PSI [3,4]. It is planned to measure the strong interaction width and shift of the ground state at the percent level. These measurements can then be used to directly extract from data the πN scattering amplitude at threshold. The aim of the experiment goes, however, further: it intends to extract from these measurements the S -wave πN scattering lengths $a_{0+}^+ + a_{0+}^-$ in pure QCD with high precision. In order to achieve this goal, the relation between the scattering lengths and the threshold amplitude must be known at an accuracy that matches the accuracy of the experiment. In other words, one has to remove isospin-breaking effects from the threshold amplitude with high precision, in the framework of QCD+QED.

Isospin-breaking effects in low-energy πN scattering have been extensively discussed in the literature on the basis of a potential model approach. The discussion relevant to the problem of pionic hydrogen can be found in Refs. [6, 7]. Here, we rely on the effective theory of QCD+QED, a method already invoked [8,9,10,11] in the analogous program for the $\pi^+\pi^-$ atom investigated presently at CERN [2]. For a critical comparison between the potential model and the effective theory framework, we refer the reader to Ref. [12].

In the case of pionic hydrogen considered here, the relation between the strong energy-level shift ϵ_{1s} of the ground state and the threshold π^-p scattering amplitude has been worked out in the effective theory in Ref. [13],

$$\epsilon_{1s} = -\frac{\alpha^3 \mu_c^3 \mathcal{T}_{\pi N}}{2\pi M_\pi} \left\{ 1 - \frac{\alpha(\ln \alpha - 1) \mu_c^2 \mathcal{T}_{\pi N}}{2\pi M_\pi} \right\} + \dots \quad (1.1)$$

Here, $\mu_c = m_p M_\pi (m_p + M_\pi)^{-1}$ denotes the reduced mass¹ of the π^-p system, and $\mathcal{T}_{\pi N}$ is the threshold amplitude for the process $\pi^-p \rightarrow \pi^-p$, evaluated at next-to-leading order in isospin breaking. Furthermore, $\alpha \simeq 1/137.036$ denotes the fine-structure constant, and the ellipsis stands for the higher-order terms in isospin breaking (see below). In the isospin symmetry limit, the threshold amplitude is proportional to a particular combination of the S -wave pion-nucleon scattering lengths a_{0+}^\pm (we use the notation of Ref. [14]),

$$\begin{aligned} \mathcal{T}_{\pi N} &= \mathcal{T}_{\pi N}^0 + \alpha \mathcal{T}^\gamma + (m_d - m_u) \mathcal{T}^m, \\ \mathcal{T}_{\pi N}^0 &= 4\pi \left(1 + \frac{M_\pi}{m_p} \right) (a_{0+}^+ + a_{0+}^-) . \end{aligned} \quad (1.2)$$

The isospin breaking amplitudes $\mathcal{T}^{\gamma,m}$ depend on the renormalization group invariant scale of QCD, and on the quark mass $\hat{m} = (m_u + m_d)/2$ (we consider two-flavor QCD). Once $\mathcal{T}^{\gamma,m}$ are calculated, a measurement of the shift ϵ_{1s} allows one to determine the combination $a_{0+}^+ + a_{0+}^-$. Similarly, a width measurement of the ground state provides $|a_{0+}^-|$. The values of these scattering lengths are correlated e.g. with the pion-nucleon sigma-term [15], with the pion-nucleon coupling constant [16], and with the Goldberger-Treiman relation, which relates the pion-nucleon coupling constant to the axial charge. It goes without saying that the scattering lengths are therefore very central objects in the analysis of pion-nucleon reactions. We refer the reader to [4] for a recent investigation of these questions. Here, we concentrate on the evaluation of the isospin breaking amplitudes $\mathcal{T}^{\gamma,m}$.

The amplitudes $\mathcal{T}^{\gamma,m}$ can e.g. be evaluated in the framework of chiral perturbation theory. Writing the energy shift in the form

$$\epsilon_{1s} = -2\alpha^3 \mu_c^2 (a_{0+}^+ + a_{0+}^-)(1 + \delta_\epsilon), \quad (1.3)$$

the leading order calculation [13] gives $\delta_\epsilon = (-4.8 \pm 2.0) \cdot 10^{-2}$, whereas the calculation by Ref. [6] in a potential model framework leads to $\delta_\epsilon = (-2.1 \pm 0.5) \cdot 10^{-2}$. How should the two calculations be compared? As has been pointed out in Ref. [13], the leading order terms in the effective theory are due to effects that are not all consistently taken into account in the potential model calculation. On the other hand, as has been emphasized in footnote 1 in Ref. [4], mass splitting effects in strong loops and γn intermediate states show up only at higher orders

in the chiral expansion. It is the aim of the present article to carry out the calculation of \mathcal{T}^γ and \mathcal{T}^m at next-to-leading order, where these effects come into play. Further, the interference effect between vacuum polarization and strong interactions will be taken into account as well² - they occur formally at next-to-next-to leading order in isospin breaking.

Isospin breaking effects in πN scattering have been studied already previously [see Ref. [17] and references therein] by using heavy baryon chiral perturbation theory (HBChPT). We were not able to directly use these results, for the following reason. In Ref. [17], the authors calculate physical amplitudes in different channels, and study combinations thereof that vanish in the isospin symmetry limit. This is not what is needed for pionic hydrogen, where one has to extract isospin-breaking correction to a single amplitude (π^-p elastic amplitude, in the case of the energy levels). Ref. [17] does not provide explicit expressions for the physical amplitudes, and we have therefore performed an independent calculation.

In Ref. [17], HBChPT was used to calculate the amplitudes. Here, we rely on the framework developed by Becher and Leutwyler [18]. This method is manifestly Lorentz invariant and preserves chiral power counting in the case where baryons and Goldstone bosons are running in the loops. In the present context, contributions from virtual photons are needed as well. We show that the method proposed in Ref. [18] can straightforwardly be adapted to this case. Individual Feynman diagrams contain ultraviolet (infrared) singularities, due to integration over large (small) momenta. We use dimensional regularization to tame both of these singularities. The counterterms from the higher order chiral Lagrangians cancel the ultraviolet poles at $d = 4$ in the final result. In order to check this cancellation, we evaluate the 1-loop divergences also with the heat-kernel method. Finally, infrared divergences disappear in physical quantities at the end of the calculation. In our case, this concerns the $\pi^-p \rightarrow \pi^-p$ scattering amplitude at threshold, with the Coulomb singularity removed. Lack of phase space forbids the emission of soft photons, as a result of which the elastic scattering amplitude must be infrared finite at threshold. Needless to say that this cancellation serves as another welcome check on our calculation.

The final result for δ_ϵ contains, at the next-to-leading order considered here, several low-energy constants (LECs) that parameterize the structure of the effective theory at this order. All but one of these LECs are under experimental control or expected to generate a small effect. The remaining one, f_1 , enters the expression already at leading order [13]. Whereas this constant is expected to contribute sizeably to δ_ϵ , no precise determination in terms of experimental data is available yet. We shall explain why, in our opinion, a precise determination of $a_{0+}^+ + a_{0+}^-$ from a measurement of the energy-level shift ϵ_{1s} has to await a corresponding precise determination of

¹ We denote the charged pion mass (the proton mass) with $M_\pi (m_p)$.

² We are indebted to T. Ericson for pointing out to us that this may be an important effect.

f_1 , and more importantly, why potential models are not of help in this respect.

The layout of the paper is as follows. In section 2 we introduce the definition of the threshold scattering amplitude in the presence of photons, and give the relation of this quantity to the strong energy shift of the π^-p atom. In section 3 we display the set of the meson and meson-nucleon chiral Lagrangians, which are used in the calculations of the threshold scattering amplitude at $O(p^3)$. In section 4 we calculate the tree-level contributions to the threshold amplitude at $O(p^3)$. In sections 5 and 6, we outline the generalization of the infrared regularization procedure [18], needed in the presence of virtual photons. The general procedure for the calculation of the S -matrix elements in the infrared regularization in the presence of virtual photons is described in section 7, where we also discuss the separation of infrared and ultraviolet divergences. Section 8 deals with the calculation of the vertex diagram with virtual photons. Here, we demonstrate the origin of the Coulomb phase and the singular piece of the scattering amplitude at threshold. In section 9 we present the final result of our calculations of the threshold amplitude, and in section 10 we discuss the size of the relevant low-energy constants. In section 11, we evaluate the ground-state energy-level shift numerically and compare the result with model calculations. Section 12 contains our summary and conclusions. Technical details are relegated to the appendices.

2 Threshold amplitude and the strong energy-level shift

It is both conventional and convenient to split the ground-state energy into electromagnetic and strong parts,

$$E_{1s} = E_{1s}^{\text{em}} + \epsilon_{1s}. \quad (2.1)$$

Despite the fact that this splitting cannot be understood literally (e.g. there are contributions from strong interactions in E_{1s}^{em}), it turns out to be useful in the theoretical analysis of hadronic atom data.

The electromagnetic part E_{1s}^{em} has been worked out in Refs. [6,13]. The results of these two investigations - that were performed in completely different settings - agree numerically with high precision. The complete analytic result of the electromagnetic energy at $O(\alpha^4)$, which is given in Ref. [13], includes relativistic corrections, finite-size effects from proton and pion charge radii, and the correction due to the anomalous magnetic moment of the proton. In addition, it includes the contribution from the electron vacuum polarization, which arises formally at $O(\alpha^5)$, but is amplified by a large coefficient $(M_\pi/m_e)^2$. The evaluation of E_{1s}^{em} in Ref. [6] includes in addition some higher-order corrections (vertex corrections, corrections to the vacuum polarization contribution), that were omitted in Ref. [13]. Numerically, however, they are much smaller than the ones included in both approaches.

What is exactly measured in the experiment at PSI, is the transition energy E_{3p-1s}^{meas} between the $3p$ and $1s$

states [3,4]. Since the electromagnetic shifts of both levels are known to a very high precision [6], and since the strong shift in the $3p$ state is very small, the measurement allows one to directly extract the strong shift of the $1s$ level according to

$$\epsilon_{1s} = E_{3p-1s}^{\text{em}} - E_{3p-1s}^{\text{meas}}. \quad (2.2)$$

The aim of the new experiment at PSI is to measure ϵ_{1s} at the percent level [3]. Once this measurement is performed, one is faced with the task of extracting the strong S -wave πN scattering lengths $a_{0+}^+ + a_{0+}^-$ from this quantity.

In order to formulate the problem rigorously, it is convenient to introduce a common counting rule for the isospin-breaking effects, parameterized by the fine structure constant α and the up and down quark mass difference $m_d - m_u$. We have found it useful to count these effects at the same order, introducing the formal parameter $\delta \sim \alpha \sim m_d - m_u$. Equation (1.1), which relates the strong shift ϵ_{1s} to the threshold amplitude, is then valid [13] up to and including terms of order δ^4 - hereafter, this is referred to as the “next-to-leading order in isospin breaking”. In the following, it is useful to introduce the notation

$$\begin{aligned} \mathcal{T}_{\pi N} &= \mathcal{T}_{\pi N}^0 + \delta\mathcal{T}, \\ \delta\mathcal{T} &= \alpha\mathcal{T}^\gamma + (m_d - m_u)\mathcal{T}^m. \end{aligned} \quad (2.3)$$

The isospin-symmetric part $\mathcal{T}_{\pi N}^0$ refers to pure QCD, where the pion and the nucleon masses are equal, by convention, to the charged pion and to the proton masses, respectively. From Eqs. (1.1), (1.2) and (1.3), the expression for the isospin-breaking correction δ_ϵ can now be readily worked out. One still has to add the correction $\delta_\epsilon^{\text{vac}}$ due to the interference of vacuum polarization and strong interactions. The complete expression takes the form

$$\begin{aligned} \delta_\epsilon &= \frac{\delta\mathcal{T}}{4\pi(1 + M_\pi/m_p)(a_{0+}^+ + a_{0+}^-)} + K + \delta_\epsilon^{\text{vac}}, \\ K &= -2\alpha(\ln \alpha - 1)\mu_c(a_{0+}^+ + a_{0+}^-). \end{aligned} \quad (2.4)$$

The only unknown ingredient in Eq. (2.4) is thus the isospin-breaking part $\delta\mathcal{T}$ of the threshold amplitude. The chiral expansion of the amplitudes \mathcal{T}^γ and \mathcal{T}^m is performed in the variable $r = M_\pi/m_p$ - the expansion of $\delta\mathcal{T}$ therefore starts at order p^2 (counting α and $m_d - m_u$ as $O(p^2)$, as usual),

$$\delta\mathcal{T} = \delta\mathcal{T}_2 + \delta\mathcal{T}_3 + O(p^4). \quad (2.5)$$

The leading term $\delta\mathcal{T}_2$ has been determined in Ref. [13]. Here, we evaluate $\delta\mathcal{T}_3$, which amounts to a one-loop calculation of the $\pi^-p \rightarrow \pi^-p$ amplitude. We will show below, that the chiral expansion of \mathcal{T}^m starts at $O(r^2)$. At the accuracy we are concerned with here, the quark mass difference does thus not enter. [The effect coming from the insertion of the quark mass difference into loops may be non-negligible [19]. Its evaluation requires the calculation of the threshold amplitude at order p^4 , which is beyond the scope of this work.]

The contribution $\delta_\epsilon^{\text{vac}}$ has been omitted in Ref. [13], since formally it is higher order in the parameter δ . However, numerically it is not negligible, because of the large coefficient containing M_π/m_e . The calculation of this correction within a non-relativistic effective Lagrangian approach has been carried out in Ref. [20]. Here, we use this result, contained in table II of Ref. [20],

$$\delta_\epsilon^{\text{vac}} = 2 \frac{\delta\Psi(0)}{\Psi(0)} = 0.48 \% , \quad (2.6)$$

where $\Psi(0)$ stands for the pionic hydrogen wave function at the origin, and where $\delta\Psi(0)$ denotes the correction to this wave function due to vacuum polarization. The result (2.6) agrees perfectly with the value $\delta_\epsilon^{\text{vac}} = 0.46 \%$ obtained within the potential model of Ref. [6].

We now present the exact definition of the threshold amplitude $\mathcal{T}_{\pi N}$ which enters the expression (1.1) for the strong energy shift of the ground state. Let us consider the elastic scattering process $\pi^-(q) + p(p) \rightarrow \pi^-(q') + p(p')$ in the vicinity of the physical threshold, at first order in the fine structure constant α . External momenta are on the mass shell $p^2 = p'^2 = m_p^2$, $q^2 = q'^2 = M_\pi^2$. The Mandelstam variables are defined in the standard manner, $s = (p + q)^2 = (p' + q')^2$, $t = (p - p')^2 = (q - q')^2$, $u = (p - q')^2 = (p' - q)^2$, $s + t + u = 2(m_p^2 + M_\pi^2)$. The 3-momentum of the pion and of the nucleon in the CM frame is given by $|\mathbf{p}| = \lambda^{1/2}(s, m_p^2, M_\pi^2)/(2\sqrt{s})$, where $\lambda(x, y, z) = (x - y - z)^2 - 4yz$ denotes the triangle function. The scattering angle is given by $\cos\theta = 1 + t/(2\mathbf{p}^2)$.

The scattering amplitude for this process can be expressed in terms of two scalar functions D and B ,³

$$T_{\pi N} = \bar{u}(p') \left\{ D(s, t) - \frac{1}{4m_p} [\not{q}', \not{q}] B(s, t) \right\} u(p),$$

$$\bar{u}(p)u(p) = 2m_p. \quad (2.7)$$

In the context of the energy-shift considered here, only the amplitude $D(s, t)$ is relevant. In the next step, we define the truncated amplitude \bar{D} , which is obtained from the scattering amplitude (2.7) by subtracting the one-photon exchange contribution displayed in Fig. 1,

$$\bar{D}(|\mathbf{p}|, \cos\theta) \doteq \bar{D}(s, t) = D(s, t) - \frac{e^2 F_\pi(t) F_1(t)(s - u)}{2m_p t}, \quad (2.8)$$

where $F_\pi(t)$ and $F_1(t)$ denote the pion electromagnetic form factor and the nucleon Dirac form factor, respectively.

³ It is well known that the above scattering amplitude in the presence of electromagnetic interactions is infrared-singular in perturbation theory. In this paper we use dimensional regularization to tame both, infrared (IR) and ultraviolet (UV) divergences. Thus, the scattering amplitudes D and B in Eq. (2.7) are meant to be evaluated at $d \neq 4$ (see below). We use the notation of Bjorken-Drell [21] for the Dirac matrices.

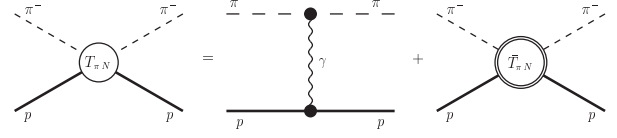


Fig. 1. Definition of the truncated $\pi^- p \rightarrow \pi^- p$ amplitude. The filled vertexes in the diagram with the photon exchange correspond to vector form factors of the pion and of the proton, calculated in pure QCD. $\bar{T}_{\pi N}$ corresponds to the truncated amplitude.

In the presence of virtual photons, at order α , the scattering amplitude $\bar{D}(|\mathbf{p}|, \cos\theta)$ contains Coulomb singularities at the physical threshold [13, 11]. In particular, there emerges the Coulomb phase which is divergent in physical dimensions $d = 4$ (cf with [22]),

$$\theta_C(|\mathbf{p}|) = \frac{\mu_c}{|\mathbf{p}|} \mu^{d-4} \left\{ \frac{1}{d-4} - \frac{1}{2} (\Gamma'(1) + \ln 4\pi) + \ln \frac{2|\mathbf{p}|}{\mu} \right\}. \quad (2.9)$$

Here μ stands for the scale in dimensional regularization.

After removing the Coulomb phase, the behavior of the real part of the amplitude $\bar{D}(|\mathbf{p}|, \cos\theta)$ in the vicinity of threshold, at order α , is given by [13]

$$\begin{aligned} & \text{Re} \left\{ e^{-2i\alpha\theta_C(|\mathbf{p}|)} \bar{D}(|\mathbf{p}|, \cos\theta) \right\} \Big|_{|\mathbf{p} \rightarrow 0} \\ &= \frac{B_1}{|\mathbf{p}|} + B_2 \ln \frac{|\mathbf{p}|}{\mu_c} + \mathcal{T}_{\pi N} + O(|\mathbf{p}|), \end{aligned} \quad (2.10)$$

where the quantities B_1 , B_2 can be related to the S -wave πN scattering lengths (their explicit form is not needed in the applications to the hadronic atom problem). The quantity $\mathcal{T}_{\pi N}$, which is referred to in this article as the *threshold scattering amplitude*, is infrared finite. It determines ϵ_{1s} according to Eq. (1.1), and is the central object of our investigation.

3 Lagrangians

In this section, we display the low-energy effective Lagrangians which are used in the calculation of the $\pi^- p$ amplitude. In particular, we provide the meson-nucleon Lagrangian at order $e^2 p$, whose divergences are consistent with the “standard” choice of the meson $O(p^4)$ [23], $O(e^2 p^2)$ [24], and nucleon $O(p^3)$ [25, 26] Lagrangians. The reason for doing so is that the $O(e^2 p)$ Lagrangian which is available in the literature [19, 27, 28], is not consistent with this choice. The details of the derivation, which was

performed by using the Berezinian approach [29,30], can be found in appendix B. In this appendix, we in addition give the relation between two sets of the LECs which are defined by the choice of the $O(p^4)$ meson Lagrangian either in form of Ref. [23], or Ref. [31].

The full Lagrangian consists of meson and nucleon parts, as well as the free photon Lagrangian together with the gauge-fixing term,

$$\begin{aligned}\mathcal{L}_{eff} &= \mathcal{L}_\pi + \mathcal{L}_N + \mathcal{L}_\gamma, \\ \mathcal{L}_\pi &= \mathcal{L}_\pi^{(p^2)} + \mathcal{L}_\pi^{(e^2)} + \mathcal{L}_\pi^{(p^4)} + \mathcal{L}_\pi^{(e^2 p^2)} + \dots, \\ \mathcal{L}_N &= \mathcal{L}_N^{(p)} + \mathcal{L}_N^{(p^2)} + \mathcal{L}_N^{(e^2)} + \mathcal{L}_N^{(p^3)} + \mathcal{L}_N^{(e^2 p)} + \dots,\end{aligned}\quad (3.1)$$

where

$$\begin{aligned}\mathcal{L}_\pi^{(p^2)} + \mathcal{L}_\pi^{(e^2)} + \mathcal{L}_\gamma &= \frac{F^2}{4} \langle d^\mu U^\dagger d_\mu U + \chi^\dagger U + U^\dagger \chi \rangle \\ &+ Z F^4 \langle Q U Q U^\dagger \rangle - \frac{1}{4} F_{\mu\nu} F^{\mu\nu} - \frac{1}{2a} (\partial_\mu A^\mu)^2, \\ \mathcal{L}_\pi^{(p^4)} &= \sum_{i=1}^7 l_i O_i^{(p^4)}, \quad \mathcal{L}_\pi^{(e^2 p^2)} = F^2 \sum_{i=1}^{10} k_i O_i^{(e^2 p^2)}, \\ \mathcal{L}_N^{(p)} &= \bar{\Psi} (i \not{D} - m + \frac{1}{2} g_A \not{A} \gamma_5) \Psi, \\ \mathcal{L}_N^{(p^2)} &= \sum_{i=1}^7 c_i \bar{\Psi} O_i^{(p^2)} \Psi, \quad \mathcal{L}_N^{(e^2)} = F^2 \sum_{i=1}^3 f_i \bar{\Psi} O_i^{(e^2)} \Psi, \\ \mathcal{L}_N^{(p^3)} &= \sum_{i=1}^{23} d_i \bar{\Psi} O_i^{(p^3)} \Psi, \quad \mathcal{L}_N^{(e^2 p)} = F^2 \sum_{i=1}^{12} g_i \bar{\Psi} O_i^{(e^2 p)} \Psi,\end{aligned}\quad (3.2)$$

where $\langle A \rangle$ denotes the trace of the matrix A . The building blocks for the mesonic Lagrangians are

$$\begin{aligned}d_\mu U &= \partial_\mu U - i \mathcal{R}_\mu U + i U \mathcal{L}_\mu, \\ \begin{pmatrix} \mathcal{R}_\mu \\ \mathcal{L}_\mu \end{pmatrix} &= v_\mu \pm a_\mu + \mathcal{Q} A_\mu, \\ \mathcal{R}_{\mu\nu} &= \partial_\mu \mathcal{R}_\nu - \partial_\nu \mathcal{R}_\mu - i [\mathcal{R}_\mu, \mathcal{R}_\nu], \\ \mathcal{L}_{\mu\nu} &= \partial_\mu \mathcal{L}_\nu - \partial_\nu \mathcal{L}_\mu - i [\mathcal{L}_\mu, \mathcal{L}_\nu], \\ \mathcal{F}_\pm^{\mu\nu} &= u^\dagger \mathcal{R}^{\mu\nu} u \pm u \mathcal{L}^{\mu\nu} u^\dagger, \\ \hat{\mathcal{F}}_\pm^{\mu\nu} &= \mathcal{F}_\pm^{\mu\nu} - \frac{1}{2} \langle \mathcal{F}_\pm^{\mu\nu} \rangle, \\ \chi &= 2B(s + ip), \quad d_\mu \chi = \partial_\mu \chi - i \mathcal{R}_\mu \chi + i \chi \mathcal{L}_\mu, \\ \mathcal{Q}_\pm &= \frac{1}{2} (u \mathcal{Q} u^\dagger \pm u^\dagger \mathcal{Q} u), \\ \mathcal{C}_R^\mu &= -i [\mathcal{R}_\mu, \mathcal{Q}], \quad \mathcal{C}_L^\mu = -i [\mathcal{L}_\mu, \mathcal{Q}],\end{aligned}$$

$$\mathcal{C}_\pm^\mu = \frac{1}{2} (u \mathcal{C}_L^\mu u^\dagger \pm u^\dagger \mathcal{C}_R^\mu u), \quad (3.4)$$

where U is a unitary 2×2 matrix, and Ψ is the nucleon field. As usual, s, p, v_μ, a_μ denote external scalar, pseudoscalar, vector and axial fields, B is a constant related to the quark condensate, and $\mathcal{Q} = e \text{diag}(\frac{2}{3}, -\frac{1}{3})$ is the quark charge matrix. The axial source is taken traceless, $\langle a_\mu \rangle = 0$.

Building blocks for the meson–nucleon Lagrangians in the presence of virtual photons are

$$\begin{aligned}D_\mu &= \partial_\mu + \Gamma_\mu, \quad U = u^2, \quad u_\mu = i u^\dagger d_\mu U u^\dagger, \\ \Gamma_\mu &= \frac{1}{2} [u^\dagger, \partial_\mu u] - \frac{i}{2} u^\dagger R_\mu u - \frac{i}{2} u L_\mu u^\dagger, \\ \chi_\pm &= u^\dagger \chi u^\dagger \pm u \chi^\dagger u, \quad \hat{\chi}_+ = \chi_+ - \frac{1}{2} \langle \chi_+ \rangle, \\ F_{\mu\nu}^\pm &= u^\dagger R_{\mu\nu} u \pm u L_{\mu\nu} u^\dagger, \quad \hat{F}_{\mu\nu}^+ = F_{\mu\nu}^+ - \frac{1}{2} \langle F_{\mu\nu}^+ \rangle, \\ \mathcal{Q}_\pm &= \frac{1}{2} (u \mathcal{Q} u^\dagger \pm u^\dagger \mathcal{Q} u), \quad \hat{\mathcal{Q}}_\pm = \mathcal{Q}_\pm - \frac{1}{2} \langle \mathcal{Q}_\pm \rangle, \\ c_\mu^\pm &= -\frac{i}{2} (u [L_\mu, \mathcal{Q}] u^\dagger \pm u^\dagger [R_\mu, \mathcal{Q}] u),\end{aligned}\quad (3.5)$$

where $Q = e \text{diag}(1, 0)$ denotes the nucleon charge matrix, and $R_\mu, L_\mu, R_{\mu\nu}, L_{\mu\nu}$ are defined just like their pionic counterparts $\mathcal{R}_\mu, \mathcal{L}_\mu, \mathcal{R}_{\mu\nu}, \mathcal{L}_{\mu\nu}$ respectively, with \mathcal{Q} replaced by Q . We have set the charge matrices \mathcal{Q} and Q to their constant physical values, and do not consider the most general expression of the effective Lagrangians containing space-dependent spurion fields $Q_{L,R}$. Furthermore, in (3.3) we drop terms which do not contain pion fields, and terms of order e^4 .

We comment on the LECs $F, g_A, Z, c_i, f_i, \dots$. The first one, F , denotes the pion decay constant in the chiral limit, and g_A is the axial charge, again at $m_u = m_d = 0$. The quantity Z is related to the pion mass difference,

$$\begin{aligned}M_{\pi^0}^2 &= (m_u + m_d)B + O(m_q^2, e^2 m_q, e^4), \\ \Delta_\pi &= M_\pi^2 - M_{\pi^0}^2 = 2e^2 F^2 Z + O(m_q^2, e^2 m_q, e^4).\end{aligned}\quad (3.6)$$

The couplings c_i, f_i are finite, if the calculation of the loop diagrams is performed in a manner that respects chiral power counting. The divergences in the remaining LECs are given by

$$\begin{aligned}l_i &= \gamma_i \lambda + l_i^r(\mu), \quad k_i = \sigma_i \lambda + k_i^r(\mu), \\ d_i &= \frac{\beta_i}{F^2} \lambda + d_i^r(\mu), \quad g_i = \frac{\eta_i}{F^2} \lambda + g_i^r(\mu),\end{aligned}\quad (3.7)$$

where

$$\lambda = \frac{\mu^{d-4}}{16\pi^2} \left(\frac{1}{d-4} - \frac{1}{2} [\Gamma'(1) + \ln 4\pi + 1] \right). \quad (3.8)$$

In appendix A we list the operators $O_i^{(k)}$, as well as the divergent parts of the low-energy constants, and provide

references to the original literature. Since our operator basis in the mesonic sector is defined in a standard manner, numerical values of l_i^r , k_i^r can be directly taken from the existing analyses. The definition of the finite constants c_i and f_i coincides with that from Refs. [25] and [27], respectively (in the latter, the notation f_i' instead of f_i is used for the LECs in the relativistic theory). Our choice for those d_i^r that contribute to the πN scattering amplitude, corresponds to the one of Ref. [32], modulo the relations (B14), which display the effect of the different choice of the mesonic basis here and in Ref. [32]. Finally, for the reasons given in appendix B, it is not clear to us how we can compare the couplings g_i^r used here, with the ones determined in Ref. [17].

In the actual calculation of the scattering amplitude, we invoke an exponential parameterization of the matrix U ,

$$U = \exp i\pi/F, \quad \pi = \begin{pmatrix} \pi^0 & \sqrt{2}\pi^+ \\ \sqrt{2}\pi^- & -\pi^0 \end{pmatrix}, \quad (3.9)$$

and use π as an interpolating field for the pions. Further, we set

$$\chi = 2B \text{diag}(m_u, m_d), \quad (3.10)$$

and perform the calculations in the Feynman gauge $a = 1$.

4 Tree contributions

The tree contributions to the threshold scattering amplitude $\mathcal{T}_{\pi N}$ include the pseudovector Born diagrams Fig. 2, and the contributions from the counterterms in the effective Lagrangians, indicated in Fig 3. Insertions in the external lines are not displayed - they will be included through mass and wave function renormalization in section 9.

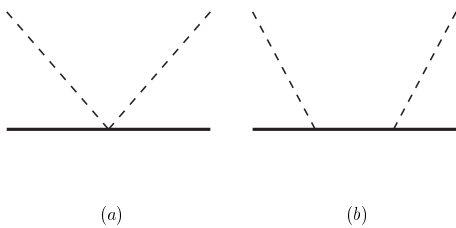


Fig. 2. The Born diagrams, vector (a) and axialvector (b) couplings.



Fig. 3. Counterterm contributions. Insertions on the external lines are not shown.

The scattering matrix elements are evaluated with meson momenta that are on the mass shell, $q^2 = q'^2 = M_\pi^2$, and with spinors that obey the Dirac equation with the physical proton mass, $\not{p}u(p, s) = m_p u(p, s)$. On the other hand, the neutron mass in the internal line in Fig 2b is the chiral symmetric one. It receives corrections from counterterm insertions ② in Fig. 3, and from the self energy diagrams s_1 and s_2 in Fig. 11. Here, we merge these contributions and evaluate the diagram Fig 2b with the physical neutron mass. [The subtraction in the one-loop self-energy-type diagrams s_1 and s_2 in Fig. 11 is then carried out on the mass shell.] In this convention, the contribution from the Born diagrams Fig.2 becomes

$$\mathcal{T}^B = \frac{M_\pi}{2F^2} - \frac{g_A^2 M_\pi^2}{2F^2(m_n + m_p + M_\pi)}. \quad (4.1)$$

Next consider the vertex corrections ① - these can be absorbed in g_A . Since they are proportional to the quark masses m_u, m_d , they do not contribute at order p^3 , and we drop them altogether. The polynomial contributions ③ arise from two-nucleon two-pion vertexes in the effective Lagrangians. We find⁴

$$\begin{aligned} \mathcal{T}^{\text{ct}} = & -\frac{4M_{\pi^0}^2}{F^2} c_1 + \frac{2M_\pi^2}{F^2} (c_2 + c_3) - \frac{e^2}{2} (4f_1 + f_2) \\ & + \frac{4M_\pi^3}{F^2} (d_1 + d_2 + d_3) + \frac{8M_\pi M_{\pi^0}^2}{F^2} d_5 \\ & + 2e^2 M_\pi (g_6 + g_8). \end{aligned} \quad (4.2)$$

5 Two-point functions of pion fields

In Ref. [18], Becher and Leutwyler have shown how power counting in baryon chiral perturbation theory (pions and nucleons running in the loops) can be incorporated in a manifestly Lorentz invariant manner. Here, we extend this framework to include virtual photons. In addition to the question of power counting, virtual photons generate the standard problems: poles in two-point functions are transformed into branch points, wave function renormalization constants become ill-defined, and truncated on-shell Green functions in general cease to exist in four

⁴ The normalization of the low-energy constants $f_{1,2}$ used in the present paper differs from that of Ref. [13]: $F^2 f_{1,2}^{\text{here}} = f_{1,2}^{\text{old}}$.

dimensions. In order to identify these infrared singularities⁵, we start the discussion of the low-energy expansion of Green functions with the two-point function of pseudoscalar quark currents. In this case, power counting does not pose a problem, because one is concerned with mesons and photons only. Furthermore, ultraviolet divergences do not show up in the final result either, because Green functions of quark currents are well defined objects in the effective Lagrangian framework. Therefore, the only obstacles in this case are the infrared divergences generated by photon loops.

5.1 Pseudoscalar two-point function

The pseudoscalar densities $P_5^\pm(x) = \bar{q}(x)i\gamma_5\tau^{1\pm i2}q(x)$ may be used as interpolating fields for the charged pions. To evaluate scattering matrix elements, the residue of the two-point function

$$G(s) = i \int dx e^{-iqx} \langle 0 | T P_5^-(x) P_5^+(0) | 0 \rangle ; \quad s = q^2 \quad (5.1)$$

at $s = M_\pi^2$ is needed - it determines the wave function renormalization constant. However, in the presence of virtual photons, G develops a branchpoint, not a pole, and that residue does not exist. There are two standard procedures to deal with the situation: Either, one introduces a photon mass, which shifts the branchpoint to $s = (M_\pi + m_\gamma)^2$, as a result of which G indeed contains a pole at the pion mass. The photon mass is then sent to zero at the very end of the relevant calculations of physical quantities. Or one instead uses dimensional regularization to tame both, ultraviolet and infrared divergences. In the following, we use the latter method. Let us consider the low energy expansion of G . Including contributions from one virtual photon as indicated in Fig. 4, and adding the counterterms from $\mathcal{L}_\pi^{(e^2 p^2)}$ in Eq. (3.1), we find

$$\begin{aligned} G(s) &= \frac{4F^2 B^2 R(s)}{M_\pi^2 - s} , \\ M_\pi^2 &= M^2 - \frac{e^2 M^2}{16\pi^2} \left\{ 3 \ln \frac{M^2}{\mu^2} - 4 \right\} \\ &\quad - e^2 M^2 K_M^r + \dots ; \quad M^2 = (m_u + m_d)B , \\ R(s) &= 1 - \frac{e^2}{8\pi^2} \left\{ r(s) + \ln \frac{M^2}{\mu^2} - 1 \right\} - e^2 K_G^r + \dots , \\ r(s) &= \frac{s + M^2}{s} \ln \frac{M^2 - s}{M^2} , \\ K_M^r &= \frac{20}{9} (k_1^r + k_2^r - k_5^r) - \frac{92}{9} k_6^r - \frac{4}{9} k_7^r - 8k_8^r , \end{aligned}$$

⁵ There are two types of infrared singularities in the present context: The ones associated with non-analytic terms in the chiral expansion, and singularities generated by the presence of photons. Since it will always be clear what singularities we have in mind, we do not distinguish in the following between the two, which makes notation less clumsy.

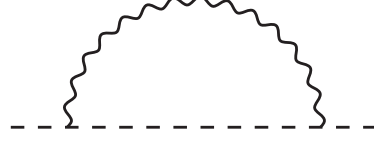


Fig. 4. Photon contribution to the two-point function of pseudoscalar fields.

$$K_G^r = \frac{20}{9} (k_1^r + k_2^r - 2k_5^r - 2k_6^r) - \frac{8}{9} k_7^r - 8k_8^r . \quad (5.2)$$

[Here, we have omitted the contributions from the leading electromagnetic term proportional to Z in Eq. (3.6), such that $M_\pi^2 = M_{\pi^0}^2$ at leading order.] The ellipses denote additional terms in the low-energy expansion. The correlator $G(s)$ is finite at nonexceptional momenta, but the residue develops a logarithmic singularity at $s = M_\pi^2$, manifest in the function $r(s)$ [at the order of the expansion considered here, we may replace M^2 in the function $r(s)$ by M_π^2].

In order to continue, we keep the dimension different from four until the very end of the calculation of physical quantities. The function $r(s)$ becomes

$$\begin{aligned} r(s, d) &= \frac{a+1}{a-1} (4\pi)^\omega \Gamma(\omega) M^{-2\omega} \int_0^1 dx x^{-\omega} \\ &\quad \times [x^{-\omega} - (1-a+ax)^{-\omega}] + O(d-4) , \\ \omega &= 2 - \frac{d}{2} , \quad a = s/M^2 . \end{aligned} \quad (5.3)$$

At nonexceptional momenta, $r(s, d)$ approaches $r(s)$ as $d \rightarrow 4$. If d is bigger than four, one may perform the mass-shell limit,

$$\begin{aligned} R(s, d) &= 1 - \frac{e^2}{8\pi^2} \left[-C_{\text{IR}}^\pi + \ln \frac{M^2}{\mu^2} \right] \\ &\quad - e^2 K_G^r + O(d-4) ; \quad s \rightarrow M_\pi^2 , \\ C_{\text{IR}}^\pi &= 2M_\pi^{d-4} \left(\frac{1}{d-4} - \frac{1}{2} (\Gamma'(1) + \ln(4\pi) + 1) \right) . \end{aligned} \quad (5.4)$$

The infrared singularity manifests itself in a pole at $d = 4$, which is due to integration over small loop momenta. We indicate the origin of this singularity with the symbol IR in the divergent quantity C_{IR}^π .

We do not use pseudoscalar densities as interpolating fields - it is simpler to use the pion fields instead. In this case, additional singularities occur at $d = 4$, as is shown in the following subsection.

5.2 Two-point function of the pion fields

The Green functions of the pion fields depend on the parameterization used for the matrix $U(x)$ in the effective Lagrangian. Here, we use the exponential parameterization (3.9), and consider the propagator of the charged fields,

$$\frac{R_\pi(s, d)}{M_\pi^2 - s} = i \int dx e^{-iqx} \langle 0 | T \pi^-(x) \pi^+(0) | 0 \rangle ; \quad s = q^2 . \quad (5.5)$$

We again include the photon loop from Fig. 4 and the pertinent counterterms from $\mathcal{L}_\pi^{(e^2 p^2)}$ at $Z = 0$. The result for the pion mass is the same as before, whereas several of the counterterms k_i are now absent in the residue. We find

$$\begin{aligned} R_\pi(s, d) &= 1 - \frac{e^2}{32\pi^2} \left[4r(s, d) + C_{UV}^\pi + 3 \ln \frac{M^2}{\mu^2} - 4 \right] \\ &- e^2 K_\pi^r + \dots , \quad K_\pi^r = \frac{20}{9} (k_1^r + k_2^r) , \\ C_{UV}^\pi &= 2M_\pi^{d-4} \left(\frac{1}{d-4} - \frac{1}{2} (\Gamma'(1) + \ln(4\pi) + 1) \right) . \end{aligned} \quad (5.6)$$

In contrast to the two-point function $G(s)$, the propagator of the pion field is ultraviolet divergent: the function R_π develops a pole in four dimensions also at nonexceptional momenta. We indicate the origin of this singularity with the symbol UV in the divergent quantity C_{UV} . The reason for the occurrence of this pole is well understood: the effective theory guarantees that Green functions of quark currents are ultraviolet finite, whereas the pion fields simply serve as integration variables in the path integral and are devoid of any physical significance.

We conclude that dimensional regularization generates two different types of poles at $d = 4$: those that are due to integrations over large loop momenta, and those that are due to considering the mass shell restriction (integrations over small loop momenta). In each graph, one may easily distinguish between the two types of singularities, and we will do so below, by denoting the corresponding singular quantities with indices UV and IR, respectively. As we shall see later, distinguishing between the two divergences serves as a powerful check on our calculation.

Later in this article, we also need the contributions from the pion loops displayed in Fig. 5. Including also the terms generated by the leading electromagnetic term proportional to Z which contributes to the pion mass difference, we find

$$\begin{aligned} Z_\pi &= R_\pi(M_\pi^2, d) = 1 + \frac{e^2}{8\pi^2} (C_{IR}^\pi - C_{UV}^\pi) \\ &+ \frac{1}{24\pi^2 F^2} (M_\pi^2 - e^2 F^2 Z) C_{UV}^\pi - \frac{e^2 Z}{24\pi^2} \\ &- \frac{20 e^2}{9} (k_1 + k_2) + O(e^2 M^2, M^4, e^4) + O(d-4) . \end{aligned}$$



Fig. 5. Pion loop contributions to the two-point function (5.5). Neutral and charged pions are running in the loop.

(5.7)

Here, it is convenient to use the unrenormalized couplings $k_{1,2}$.

6 Two-point function of baryon fields

6.1 Self-energy of the heavy scalar field

We now consider the case where a heavy particle interacts with the photon. To illustrate the method to preserve chiral power counting in this case, we consider the self energy diagram Fig. 6, which represents a heavy scalar particle

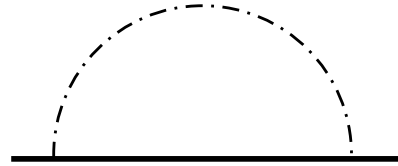


Fig. 6. Self-energy diagram for a heavy field of mass m . The solid line denotes the heavy field, and the dash-dotted line stands for a massless scalar particle.

of mass m , interacting with a massless field,

$$\begin{aligned} \Sigma(s, d) &= \frac{1}{i(2\pi)^d} \int \frac{d^d k}{[-k^2][m^2 - (p-k)^2]} \\ &= (4\pi)^{-(2-w)} \Gamma(w) \int_0^1 dx z^{-w} , \\ z &= x(m^2 - s(1-x)) ; \quad s = p^2 . \end{aligned} \quad (6.1)$$

Evaluation in the standard manner shows that Σ is of chiral order zero, $\Sigma \sim \text{const.}$, near the mass shell, whereas power counting suggests that it is of order one, $\Sigma \sim (m^2 - s)/m^2$. In Ref. [18], it has been shown that power counting with nucleon and pion fields is preserved, if one extends the integration over the Feynman parameter - that combines the heavy and light fields - from zero to infinity.

Proceeding in the same manner for photon fields, we find that

$$\begin{aligned}\Sigma^I(s, d) &= (4\pi)^{-(2-w)} \Gamma(w) \int_0^\infty dx z^{-w} \\ &= (4\pi)^{-(2-w)} \Gamma(w) \Omega^{1-2w} s^{-w} \int_0^\infty dx x^{-w} (1+x)^{-w} ; \\ \Omega &= (m^2 - s)/s ,\end{aligned}\quad (6.2)$$

where the index I denotes the infrared part à la Becher-Leutwyler. It is seen that the self energy diagram is now of chiral order one near threshold. The mass shell constraint is performed by first continuing the result to dimensions bigger than four, as before. One finds that

$$\Sigma^I(m^2, d) = \Sigma^{I'}(m^2, d) = 0 \quad , \quad d > 4 \quad , \quad (6.3)$$

where the prime denotes a derivative with respect to s . In other words, the self energy diagram Fig.6 does contribute neither to the mass nor to the residue of the two-point function in this prescription.

We found it very useful to distinguish between infrared and ultraviolet divergences also here. This may be achieved as follows. We consider the self energy and its derivative at $s = m^2$. From Eq. (6.1), one has

$$\begin{aligned}\Sigma^S(m^2, d) &= \frac{1}{16\pi^2} (-C_{UV} + 1) \quad , \\ C_K &= 2m^{d-4} \left(\frac{1}{d-4} - \frac{1}{2} (\Gamma'(1) + \ln(4\pi) + 1) \right) \quad , \\ K &= UV, IR.\end{aligned}\quad (6.4)$$

We have indicated with the index S the standard procedure, where the integral over the Feynman parameter is performed from zero to one. We have booked the singularity at $d = 4$ as an ultraviolet one for obvious reasons. The derivative is

$$\Sigma^{S'}(m^2, d) = \frac{1}{32\pi^2 m^2} (C_{IR} - 1) \quad , \quad (6.5)$$

where the singularity at $d = 4$ is now due to integrations over small momenta and therefore booked as an infrared singularity. The Becher-Leutwyler infrared regularized part is obtained by subtracting from these expressions the 'regular part' of the Feynman diagram,

$$\Sigma^R(s, d) = -(4\pi)^{-(2-w)} \Gamma(w) \int_1^\infty dx z^{-w} \quad . \quad (6.6)$$

This integral converges for $d < 3$ - the relevant poles at $d = 4$ are therefore booked as ultraviolet. We find

$$\begin{aligned}\Sigma^R(m^2, d) &= \frac{1}{16\pi^2} (-C_{UV} + 1) \quad , \\ \Sigma^{R'}(m^2, d) &= \frac{1}{32\pi^2 m^2} (C_{UV} - 1) \quad ,\end{aligned}\quad (6.7)$$

and therefore

$$\Sigma^I(m^2, d) = \Sigma^S(m^2, d) - \Sigma^R(m^2, d) = 0 \quad , \quad (6.8)$$

$$\Sigma^{I'}(m^2, d) = \frac{1}{32\pi^2 m^2} (C_{IR} - C_{UV}) \quad . \quad (6.9)$$

The result for the value of the self energy on the mass shell agrees with Eq. (6.3), whereas its derivative becomes the same upon identifying C_{IR} with C_{UV} .

6.2 The nucleon propagator

The infrared regularized nucleon propagator is evaluated in a completely analogous manner, applying infrared regularization to both, the pion and the photon field. In the following, we only need the wave function renormalization constant for the proton field. We define it in the following manner. The propagator is

$$S^{\alpha\beta}(p, d) = i \int dx e^{ipx} \langle 0 | T P^\alpha(x) \bar{P}^\beta(0) | 0 \rangle \quad , \quad (6.10)$$

where $P(x)$ denotes the proton field. The Z -factor is obtained from

$$\left\{ \lim_{p^2 \rightarrow m_p^2} (m_p - \not{p}) S(p, d) \right\} u(p, r) = Z_N u(p, r) \quad , \quad d > 4 \quad , \quad (6.11)$$

where m_p denotes the physical proton mass, $u(p, r)$ is a spinor in d dimensions with $(\not{p} - m_p)u(p, r) = 0$, and where Z_N depends on the prescription used for performing the integration over the Feynman parameters (standard, regular or infrared). We obtain for the infrared regularized Z -factor at order p^2

$$\begin{aligned}Z_N &= 1 + \frac{e^2}{8\pi^2} (C_{IR} - C_{UV}) \\ &\quad - \frac{g_A^2 m^2}{64\pi^2 F^2} \left(H_0^I + \frac{\Delta_\pi}{m^2} H_\pi^I \right) + O(p^3) \quad ,\end{aligned}\quad (6.12)$$

with

$$\begin{aligned}H_0^I &= r^2 (6 + 9 C_{UV} + 18 \ln r) \quad , \\ H_\pi^I &= -(5 + 3 C_{UV} + 6 \ln r) \quad ; \quad r = M_\pi/m \quad .\end{aligned}\quad (6.13)$$

Here, we have replaced the physical nucleon mass with its chiral limit mass m - this is correct at the order of the low-energy expansion we are working. We will do this in all loop amplitudes considered below.

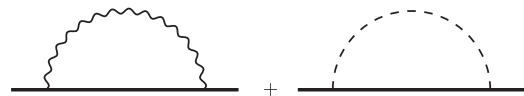


Fig. 7. Photon and pion loop contribution to the two-point function (6.10) of the proton. Neutral and charged pions are running in the loop.

7 Evaluation of S -matrix elements

Here, we describe the evaluation of the S -matrix element for the process $\pi^- p \rightarrow \pi^- p$ in this framework. The basic element to be evaluated first is the truncated four-point function

$$\langle 0 | T \pi^-(x_1) \pi^+(x_2) P^\alpha(x_3) \bar{P}^\beta(x_4) | 0 \rangle \quad (7.1)$$

in d space-time dimensions. We take into account tree graphs evaluated with \mathcal{L}_{eff} and one-loop graphs generated by $\mathcal{L}_\pi^{(p^2)}$, $\mathcal{L}_\pi^{(e^2)}$ and $\mathcal{L}_N^{(p)}$. The relevant diagrams are displayed in Figs. (2,3,9, 10,11). At the end, one multiplies the result with the incoming and outgoing spinors for the proton field, and incorporates the contribution from the wave function renormalization constants for the pion and nucleon field, determined in sections 5, 6 in the standard manner. For general momenta of the incoming and outgoing particles, the limit $d \rightarrow 4$ does not exist due to the infrared divergences which are generated by virtual photons. As we discussed in section 2, these divergences are absent in the amplitude at threshold, provided that one has removed the infrared divergent Coulomb phase. Here, we are interested in the infrared finite quantity $\mathcal{T}_{\pi N}$ defined in Eq. (2.10). The final result depends on the manner the integration over the Feynman parameters is carried out (standard, regular or infrared). Here, we work with the prescription given in Ref. [18], which preserves chiral power counting. In order to keep track of UV and IR divergences, we found it convenient to evaluate the regular part of each diagram separately, and subtract it from the same diagrams calculated in the standard manner. The procedure was illustrated in sections 5, 6 for the two-point functions. It can straightforwardly be generalized to any of the one-loop diagrams encountered here. The schematic prescription is as follows:

- i) Graphs with no virtual nucleons need no infrared regularization - graphs with closed nucleon lines vanish in infrared regularization.
- ii) Graphs with pions (or photons or both) and nucleons running in the loop, are evaluated in the following manner. Heavy (nucleons) and light (pions and photons) lines in the diagrams are combined together separately by using Feynman parameterization, as described in section 6 of Ref. [18]. The pertinent denominators are then combined with a single Feynman parameter [x attached to the heavy and $(1-x)$ to the light line]. The infrared regularization consists [18] in extending the region of integration over this parameter, from $[0, 1]$ to $[0, \infty]$.
- iii) In order to distinguish between ultraviolet and infrared divergences in graphs with a virtual photon, we evaluate the infrared regularized part as the difference between the standard and regular contribution. Symbolically,

$$\begin{aligned} M^I &= \int_0^\infty dx F = M^S - M^R, \\ M^S &= \int_0^1 dx F, \quad M^R = - \int_1^\infty dx F. \end{aligned} \quad (7.2)$$

Here, M^I stands for the final result of the calculation of any diagram in the infrared regularization, and F denotes the corresponding integrand, where the integration over the remaining Feynman parameters is implicit.

- iv) One may clearly distinguish UV and IR divergences in the one-loop diagrams which are contained in M^S , see sections 5, 6. All divergences in M^R at $d \rightarrow 4$ are declared to be ultraviolet. At the end, all infrared divergences cancel in $\mathcal{T}_{\pi N}$. Ultraviolet divergences of the one-loop diagrams cancel against the divergent parts of the low-energy constants, as a result of which the quantity $\mathcal{T}_{\pi N}$ is IR and UV finite.

The calculations may be simplified considerably if one makes use of the fact that power counting is now preserved: Nucleon (meson) propagators count as p^{-1} (p^{-2}). The numerators can then be simplified by dropping terms that generate contributions beyond the order p^3 considered here. The procedure is described in [32]. Here, one may use in addition that we work at threshold, where the pion momenta are proportional to the nucleon momenta, $p'^\mu = p^\mu$, $q'^\mu = q^\mu = p^\mu M_\pi / m_p$. Examples of such simplifications are given in section 8, where the triangle diagram is evaluated.

We add a comment on the quark mass difference $\Delta = m_d - m_u$ that occurs in the isospin violating part of the threshold amplitude. It shows up in two ways: first, through the neutron and proton masses in Feynman diagrams, and second, through vertexes in the effective Lagrangian. Consider first the latter contributions. From Eq. (4.1), it is explicitly seen that Δ does not occur at order p^3 , once the physical masses are used in the tree diagram Fig.2b. Further, in Eq. (4.1), we may replace the neutron mass by the proton mass at order p^3 - Δ still does not occur. Next consider loop diagrams, which are evaluated with the nucleon masses in the chiral limit, $m_p = m_n = m$, and are of order p^3 in the framework used here. Therefore, Δ cannot contribute. [Note that there is a difference between the nucleon and pion masses in this respect: The electromagnetic contribution to the charged pion mass is of the same order in the chiral counting as the leading term. Therefore, it matters what pion is running in the loop.] We conclude that the amplitude \mathcal{T}^m in (1.2) is of order M_π^2 and therefore beyond the accuracy of the calculation considered here.

8 The triangle diagram

In this section we investigate the infrared-divergent Coulomb phase, as well as the singular terms in the real part of the amplitude that behave like $|\mathbf{p}|^{-1}$ in the vicinity of the physical threshold. At one loop, these factors arise when one calculates radiative corrections to the strong tree-level amplitudes which are obtained from the nucleon Lagrangian $\mathcal{L}_N^{(p)}$. For illustration, we consider the strong diagram emerging from the Weinberg-Tomozawa (WT) vertex (Fig. 2a). The scattering amplitude corre-

sponding to this diagram is

$$T_{WT} = \bar{u}(p') \frac{\not{q} + \not{q}'}{4F^2} u(p). \quad (8.1)$$

The Coulomb singularities arise when one considers the virtual photon corrections to this vertex with a particular topology (v_1), depicted in Fig. 9. There are two diagrams of this type, with the photon emitted and absorbed either in the initial or in the final state. The contributions of these diagrams to the amplitude at threshold are the same, so it suffices to consider one of them, and multiply the result by 2. The total contribution of these diagrams is

$$T_{v_1} = \frac{e^2}{2F^2} \int \frac{d^d k}{(2\pi)^d} \frac{\bar{u}(p')(\not{q} + \not{q}' - \not{k})}{[-k^2]} \times \frac{(m + \not{p} + \not{k})(2\not{q} - \not{k})u(p)}{[m^2 - (p + k)^2][M_\pi^2 - (q - k)^2]}. \quad (8.2)$$

The numerator can be rewritten in the following manner,

$$\begin{aligned} & \bar{u}(p')(\not{q} + \not{q}' - \not{k})(m + \not{p} + \not{k})(2\not{q} - \not{k})u(p) = \\ & \bar{u}(p') \left\{ (2(\not{q} + \not{q}') - \not{k})[m^2 - (p + k)^2] \right. \\ & \left. + 4\not{q}'(m + \not{p})\not{q} + 4\not{q}'\not{k}\not{q} \right\} u(p). \end{aligned} \quad (8.3)$$

According to the discussion in section 7, we drop here the last term that does not contribute to the amplitude at $O(e^2 p)$. Then, after some algebra, one arrives at the following expression for the sum of contributions of tree (WT) and one-loop (v_1) diagrams to the invariant amplitude D given by Eq. (2.7),

$$D_{WT} + D_{v_1} = \frac{s - u}{8mF^2} \left\{ 1 + e^2 \left[\frac{J_1}{2M_\pi^2} + 4J_2 + 4(s - m^2)J_\gamma(s) \right] \right\} + \dots, \quad (8.4)$$

where the ellipsis stands for higher-order terms in the chiral expansion. The scalar integrals that enter the expression (8.4), are given by

$$\begin{aligned} J_1 &= \int \frac{d^d k}{(2\pi)^d} \frac{1}{M_\pi^2 - k^2} = \frac{M_\pi^2}{16\pi^2} C_{UV}^\pi, \\ J_2 &= \int \frac{d^d k}{(2\pi)^d} \frac{1}{[-k^2][M_\pi^2 - (q - k)^2]} \\ &= -\frac{1}{16\pi^2} (C_{UV}^\pi - 1), \\ J_\gamma(s) &= \int \frac{d^d k}{(2\pi)^d} \frac{1}{[-k^2][m^2 - (p + k)^2][M_\pi^2 - (q - k)^2]}. \end{aligned} \quad (8.5)$$

The representation (8.4) turns out to be very convenient to study the threshold behavior of the amplitude. The reason for this is that the integral $J_\gamma(s)$ enters here with a

coefficient which counts at $O(e^2 p^2)$ - so, the regular part of $J_\gamma(s)$, which is a polynomial in the external momenta and masses, cannot contribute at $O(e^2 p)$ to the amplitude D . Consequently, one may use the standard dimensional regularization instead of infrared regularization for calculating this integral.

Introducing Feynman parameters, the momentum integration in $J_\gamma(s)$ can be explicitly done,

$$\begin{aligned} J_\gamma(s) &= \frac{\Gamma(3 - \frac{d}{2})}{(4\pi)^{d/2}} \int_0^1 d\alpha_1 d\alpha_2 d\alpha_3 \\ &\times \delta\left(1 - \sum_{i=1}^3 \alpha_i\right) [J(\alpha)]^{d/2-3}, \\ J(\alpha) &= (\alpha_1 + \alpha_2)(\alpha_1 m^2 + \alpha_2 M_\pi^2) - \alpha_1 \alpha_2 s. \end{aligned} \quad (8.6)$$

One may single out the infrared divergence at $d = 4$ by rescaling the Feynman parameters according to $\alpha_{1,2} \rightarrow (1 - \alpha_3)\alpha_{1,2}$ - the integration over the parameter α_3 then factorizes, and we arrive at the following expression,

$$\begin{aligned} J_\gamma(s) &= \frac{1}{32\pi^2 m^2} \left\{ (C_{IR} + 1) \int_0^1 \frac{d\alpha_1}{R} + \int_0^1 \frac{d\alpha_1 \ln R}{R} \right\}, \\ R &= \alpha_1 + (1 - \alpha_1)r^2 - \alpha_1(1 - \alpha_1)\bar{s}, \quad \bar{s} = \frac{s}{m^2}. \end{aligned} \quad (8.7)$$

Using the formulae (C2), (C4) from appendix C, and expanding near threshold, for the sum $D_{WT} + D_{v_1}$ we finally obtain

$$\begin{aligned} D_{WT} + D_{v_1} &= \frac{M_\pi}{2F^2} \left\{ 1 + 2i\alpha\theta_C(|\mathbf{p}|) + \frac{\pi\alpha\mu_c}{|\mathbf{p}|} \right. \\ &\quad \left. + \frac{\alpha}{\pi r} I_V^1 + O(|\mathbf{p}|) \right\}, \\ I_V^1 &= -\frac{r}{8} (7C_{UV} + 8C_{IR} + 30 \ln r + 16) + O(r^2); \\ r &= \frac{M_\pi}{m}, \end{aligned} \quad (8.8)$$

where the Coulomb phase $\theta_C(|\mathbf{p}|)$ is given in Eq. (2.9).

From Eq. (8.8) it is evident, that the combination $\exp^{-2i\alpha\theta_C(|\mathbf{p}|)} (D_{WT} + D_{v_1})$ [cf with Eq. (2.10)] does not contain the Coulomb phase at $O(\alpha)$. Further, dropping the term proportional to $|\mathbf{p}|^{-1}$, one may read off the corresponding contribution I_V^1 to the threshold amplitude $\mathcal{T}_{\pi N}$, see table 6, entry (v_1). Finally, we note that in the amplitude there is no term that behaves like $\ln |\mathbf{p}|$ near threshold - the coefficient B_2 in Eq. (2.10) first appears at two-loop order [11].

9 The threshold amplitude at order p^3

We do not provide any further details of the calculations that can be done along the lines illustrated in previous sections. In this section, we combine the various pieces

and present the final expression for the threshold scattering amplitude $\mathcal{T}_{\pi N}$. This quantity is given by a sum of several contributions: to the contribution of Born diagrams Eq. (4.1), multiplied by the pion and nucleon wave function renormalization factors (Eqs. (5.7) and (6.12), respectively), one has to add the contributions from vector (Fig. 9), axial (Fig. 10) and strong (Fig. 11) loops, as well as the counterterm contribution \mathcal{T}^{ct} displayed in (4.2),

$$\mathcal{T}_{\pi N} = Z_\pi Z_N \mathcal{T}^{\text{B}} + \mathcal{T}^{\text{V}} + \mathcal{T}^{\text{A}} + \mathcal{T}^{\text{S}} + \mathcal{T}^{\text{ct}}, \quad (9.1)$$

where

$$\begin{aligned} \mathcal{T}^{\text{V}} &= \frac{e^2 m}{8\pi^2 F^2} \sum_{i=1}^6 I_V^i, & \mathcal{T}^{\text{A}} &= \frac{e^2 g_A^2 m}{32\pi^2 F^2} \sum_{i=1}^9 I_A^i, \\ \mathcal{T}^{\text{S}} &= \frac{m^3}{\pi^2 F^4} \sum_{i=1}^{24} (I_0^i + \frac{\Delta_\pi}{m^2} I_\pi^i). \end{aligned} \quad (9.2)$$

The quantities I_V^i , I_A^i , I_0^i and I_π^i , that correspond to the contributions from individual vector, axial and strong diagrams, are listed in tables 6, 7 and 8 in appendix D. Not all of the diagrams that are shown in Figs. 9, 10 and 11, do contribute to the threshold amplitude at $O(p^3)$. The diagram (s_{24}) in Fig. 11 e.g. vanishes trivially after the momentum integration. Moreover, there are two reasons for which some of the diagrams that are formally $O(p^3)$ in chiral counting, start to contribute at higher order:

- i) In the one-particle reducible diagrams Fig. 10: (a_1), (a_2), (a_5), and Fig. 11: (s_1), (s_2), (s_5), (s_6), (s_7), (s_8), (s_9), (s_{17}), the neutron propagator is followed by $\not{q}_\pi \gamma_5 u(p)$ (initial state), or preceded by $\bar{u}(p') \not{q}_\pi \gamma_5$ (final state), where q_π stands either for q or for q' . Formally, the combination [$\not{q}_\pi \gamma_5 \times$ propagator] is of chiral order zero. However, putting γ_5 through the nucleon propagator changes the sign of the nucleon momentum, and the whole expression starts to contribute at $O(p)$.
- ii) Doing the simplification of numerators in a manner described in sections 7 and 8 for the diagrams (a_3), (a_6), (a_7) and (s_3), (s_4), (s_{10}), (s_{11}), it is easy to observe that the leading-order contributions in the numerators vanish at threshold.

For this reason, in tables 6, 7 and 8 we do not display the contributions from the above-mentioned diagrams.

Adding all pieces together in the amplitude, we have checked that all UV divergences, as expected, cancel with the divergent parts of the LECs, whereas the IR divergences cancel among themselves. The final results is thus given in terms of renormalized LECs l_i^r , k_i^r , d_i^r , g_i^r . Further, we split the threshold amplitude in its isospin-conserving and isospin-violating parts according to Eq. (2.3). The expressions for these parts are given by (for convenience, we use here the physical proton mass m_p and the physical pion decay constant F_π)

$$\mathcal{T}_{\pi N}^0 = \frac{M_\pi}{2F_\pi^2} - \frac{g_A^2 M_\pi^2}{4m_p F_\pi^2} + \frac{2M_\pi^2}{F_\pi^2} (-2c_1 + c_2 + c_3)$$

$$\begin{aligned} &+ \frac{g_A^2 M_\pi^3}{8m_p^2 F_\pi^2} + \frac{M_\pi^3}{16\pi^2 F_\pi^4} \left(1 + \frac{3\pi g_A^2}{4} - 2 \ln \frac{M_\pi}{\mu} \right) \\ &+ \frac{M_\pi^3}{F_\pi^4} l_4^r + \frac{4M_\pi^3}{F_\pi^2} (d_1^r + d_2^r + d_3^r + 2d_5^r) + O(p^4), \end{aligned} \quad (9.3)$$

$$\begin{aligned} \delta\mathcal{T} &= \delta\mathcal{T}_2 + \delta\mathcal{T}_3 + O(p^4), \\ \delta\mathcal{T}_3 &= \delta\mathcal{T}_3^{\text{str}} + \delta\mathcal{T}_3^{\text{em}} + \delta\mathcal{T}_3^{\text{ct}}, \end{aligned} \quad (9.4)$$

$$\begin{aligned} \delta\mathcal{T}_2 &= \frac{4\Delta_\pi}{F_\pi^2} c_1 - \frac{e^2}{2} (4f_1 + f_2), \\ \delta\mathcal{T}_3^{\text{str}} &= -\frac{M_\pi \Delta_\pi}{32\pi^2 F_\pi^4} \left(3 + \frac{33\pi g_A^2}{4} + 2 \ln \frac{M_\pi}{\mu} \right), \\ \delta\mathcal{T}_3^{\text{em}} &= -\frac{e^2 M_\pi g_A^2}{32\pi^2 F_\pi^2} \left(2 + \pi + 8 \ln 2 + 12 \ln \frac{M_\pi}{\mu} \right), \end{aligned}$$

$$\begin{aligned} \delta\mathcal{T}_3^{\text{ct}} &= -\frac{8M_\pi \Delta_\pi}{F_\pi^2} d_5^r \\ &+ 2e^2 M_\pi \left(g_6^r + g_8^r - \frac{5}{9F_\pi^2} (k_1^r + k_2^r) \right), \end{aligned} \quad (9.5)$$

where $\delta\mathcal{T}_2$, $\delta\mathcal{T}_3$ are of order p^2 and p^3 , respectively. From the above equations one may easily check that the amplitude does not depend on the scale μ . Note that here we have replaced the pion decay constant in the chiral limit F by the physical decay constant F_π ,

$$F_\pi = F \left\{ 1 + \frac{M_\pi^2}{F^2} \left(l_4^r - \frac{1}{8\pi^2} \ln \frac{M_\pi}{\mu} \right) + O(M_\pi^4) \right\}. \quad (9.6)$$

This is the reason that l_4^r occurs in Eq. (9.3).

Equations (9.4) and (9.5) represent our main result. This is a complete calculation of the isospin-breaking part of the threshold scattering amplitude at $O(p^3)$ in relativistic baryon ChPT, by using the infrared regularization method of Refs. [18,32]. The isospin-conserving part of the amplitude, given in Eq. (9.3), agrees with the one displayed in appendix A of Ref. [33]. A calculation of isospin breaking effects at order p^3 has been performed by the same authors in [17]. Since they do not provide a complete analytic expression of the scattering amplitude, it is not possible to compare the results.

10 The size of the low-energy constants

In this section, we discuss the size of the low-energy constants that occur in the isospin breaking amplitude $\delta\mathcal{T}$. The amplitude $\delta\mathcal{T}_2$ ($\delta\mathcal{T}_3$) contains $4f_1 + f_2$, c_1 ($k_1^r + k_2^r$, $g_6^r + g_8^r$, d_5^r). We start the discussion with $\delta\mathcal{T}_2$ and consider the constant c_1 . It has been determined from threshold data [34] in Ref. [32]. The uncertainty in c_1 may be obtained from equation (20.2) in [32], using Höhler's values [14] for the uncertainties in the threshold parameters

and in the coupling constant $g_{\pi N}$. We find⁶

$$c_1 = -(0.93 \pm 0.07) \text{GeV}^{-1}. \quad (10.1)$$

For a comparison with other determinations of c_1 , see table 1 in Ref. [36].

Next, consider f_1 and f_2 that occur in the order e^2 pion-nucleon Lagrangian. Up to terms of order π^4 , that Lagrangian is

$$\begin{aligned} \mathcal{L}_N^{(e^2)} &= F^2 \bar{\Psi} O \Psi, \\ O &= \frac{e^2}{2} [(f_1 + f_3) \cdot 1_2 + f_2 \tau_3] \\ &\quad - \frac{2f_1 e^2}{F^2} \pi^+ \pi^- \cdot 1_2 + e f_2 \bar{Q} + \dots, \\ \bar{Q} &= \frac{e}{4F^2} \begin{pmatrix} -2\pi^+ \pi^- & \sqrt{2}\pi^0 \pi^+ \\ \sqrt{2}\pi^0 \pi^- & 2\pi^+ \pi^- \end{pmatrix}; \quad 1_2 = \text{diag}(1, 1), \end{aligned} \quad (10.2)$$

where τ_3 denotes the Pauli-matrix. From this decomposition, it is seen that f_1 occurs in the chiral expansion of the nucleon mass and in elastic pion-nucleon scattering $\pi^\pm p(n) \rightarrow \pi^\pm p(n)$. The electromagnetic part of the proton-neutron mass difference is given by the constant f_2 at leading order in the chiral expansion,

$$-e^2 F^2 f_2 = (m_p - m_n)^{\text{em}}. \quad (10.3)$$

Here, we disagree with the result Eq. (12) of Ref. [19] by a factor of 2. Numerically, we use $(m_p - m_n)^{\text{em}} = (0.76 \pm 0.3) \text{MeV}$ [37], or

$$f_2 = -(0.97 \pm 0.38) \text{GeV}^{-1}. \quad (10.4)$$

We are now left with the determination of f_1 . The sum $m_p + m_n$ contains the combination $e^2(f_1 + f_3)$ - the constants f_1 and f_3 can therefore not be disentangled from information on the nucleon masses. We may consider $m_p + m_n$ as a quantity that fixes f_3 , once f_1 is known. Therefore, elastic pion-nucleon scattering is the only realistically accessible source of information on f_1 . In principle, one may consider combinations of amplitudes that vanish in the isospin symmetry limit, and determine f_1 from those. The combination

$$X = T^{\pi^+ p \rightarrow \pi^+ p} + T^{\pi^- p \rightarrow \pi^- p} - 2T^{\pi^0 p \rightarrow \pi^0 p} \quad (10.5)$$

has this property. The tree graphs of X start at order p^2 and contain f_1 - that one may try to determine hence from here. Of course, one is faced with a problem of accuracy: in order to determine X , one needs to consider the difference of two large numbers, quite aside from the fact that the cross section $\pi^0 p \rightarrow \pi^0 p$ is not known experimentally. It remains to be seen whether a combination of experimental data and lattice calculations could resolve the problem also in practice.

⁶ We use for M_π, m_p, \dots in the following the values quoted in [35], in particular $F_\pi = 92.4 \text{ MeV}$, $|g_A| = 1.267$.

In the absence of precise experimental information on f_1 , we can i) rely on order-of-magnitude estimates, or ii) consider model calculations. As to order-of-magnitude estimates, we follow Fettes and Meißner [38] and write

$$F^2 e^2 |f_1| \simeq \frac{\alpha}{2\pi} m_p,$$

or

$$|f_1| \simeq 1.4 \text{GeV}^{-1}, \quad (10.6)$$

because f_1 is due to a genuine photon loop at the quark level (we divide by 2π rather than by 4π [38] to be on the conservative side). This estimate also confirms the expectation [13] that $|f_1|$ has the same size as $|f_2|$, see Eq. (10.4). As to model calculations, we refer the reader to Ref. [39], where c_1 and $f_{1,2,3}$ have been determined in a quark model, with the result

$$c_1 = -1.2 \text{GeV}^{-1},$$

$$F^2(f_1, f_2, f_3) = (-19.5 \pm 1.6, -8.7 \pm 0.7, 18 \pm 1.5) \text{MeV}. \quad (10.7)$$

Finally, we come to the low-energy constants that occur in the next-to-leading order amplitude $\delta\mathcal{T}_3$. The contributions of the relevant LECs to δ_ϵ is suppressed by one power of the pion mass with respect to the ones from c_1, f_1 and f_2 that occur at leading order - therefore, we expect their effect to be substantially smaller, because they represent polynomial parts of the amplitudes, not chiral singular pieces. The value for d_5^r is given in table 1 of Ref. [32] (we have chosen the entry with the largest uncertainty assigned)

$$16M_\pi^2 d_5^r(\mu) = 0.04 \pm 0.06 - \frac{2M_\pi^2}{F^2} l_4^r(\mu), \quad \mu = 1 \text{GeV}. \quad (10.8)$$

Here, we have translated the d_5^r from Ref. [32] into the present scheme according to Eq. (B14). Below, we will use $l_4^r(1 \text{GeV}) = 2.9 \cdot 10^{-3}$ [5]. For $k_1^r + k_2^r$, we invoke standard dimensional arguments for an estimate of its size, $|k_i^r| \simeq \frac{1}{16\pi^2}$, and apply the same rule to $g_6^r + g_8^r$,

$$|k_1^r + k_2^r| \simeq \frac{2}{16\pi^2}, \quad |g_6^r + g_8^r| \simeq \frac{2}{16\pi^2 F^2}. \quad (10.9)$$

[In Ref. [17], $g_6^r + g_8^r$ was estimated from an analysis of pion-nucleon scattering at low energies. However, in that reference, renormalization was treated in a manner different from the framework used here, and it is not clear to us how we can compare the couplings determined there with the ones used here, see appendix B.] As a check of this procedure, we apply the same estimate to d_5^r , namely $|d_5^r| \simeq \frac{1}{16\pi^2 F^2}$. Comparing with Eq. (10.8), we see that this guess is a rather generous one.

11 Ground-state energy-level shift

We are now ready to provide numerical values for the correction δ_ϵ in the strong energy-level shift δ_ϵ according to

Table 1. Individual contributions to δ_ϵ . K denotes the bound-state correction in Eq. (2.4). See text for details.

source	$\delta_\epsilon \times 10^2$	
$\delta\mathcal{T}_2 _{f_1=0}$	-5.5	
f_1	± 2.8	
	$\mu = 500 \text{ MeV}$	$\mu = 1 \text{ GeV}$
$\delta\mathcal{T}_3^{\text{str}}$	-3.5	-3.4
$\delta\mathcal{T}_3^{\text{em}}$	0.4	1.1
d_5^r	-0.3 ± 0.3	-0.2 ± 0.3
$k_1^r + k_2^r$	± 0.2	
$g_6^r + g_8^r$	± 0.4	
K	0.66	
vac. pol. [20]	0.48	

Eqs. (1.3) and (2.4). In addition to the LECs, we need the value for the scattering lengths a_{0+}^\pm . We take from Ref. [4]

$$a_{0+}^+ + a_{0+}^- = 0.0883 M_\pi^{-1} . \quad (11.1)$$

11.1 The correction δ_ϵ

The contribution from the leading term $\delta\mathcal{T}_2$ was already determined in Ref. [13]. This contribution contains the three LECs f_1 , f_2 and c_1 . For f_1 , the estimate $|f_1| < |f_2|$ was used in [13]. The corresponding contribution to δ_ϵ is $\pm 1.9 \cdot 10^{-2}$. Here, we use the estimate (10.6), which is slightly more conservative, and display in table 1 the contribution due to $\delta\mathcal{T}_2|_{f_1=0}$, f_1 and to the bound state correction K . We will use below this information to estimate the uncertainty in the final result.

The next order in the chiral expansion of δ_ϵ is obtained from the second term in (2.4), evaluated with $\delta\mathcal{T} = \delta\mathcal{T}_3$. We split this term further into contributions that stem from the photon loop, strong loops and counterterms, as indicated in (9.4). Note that the individual terms are scale dependent, whereas the full result is not, of course. In the table, we present the values obtained from the strong loops and photon loops at two values of the scale, $\mu = 500 \text{ MeV}$ and $\mu = 1 \text{ GeV}$. The contributions from the strong loops are substantial and of negative sign. This large contribution is mainly due to the three graphs Fig. 11 (s_{19}), (s_{21}) and (s_{22}), which add

$$\delta\mathcal{T}_3^{\text{str}} \Big|_{(s_{19}), (s_{21}), (s_{22})} = -\frac{33\pi g_A^2}{128\pi^2 F_\pi^4} M_\pi \Delta_\pi , \quad (11.2)$$

or $\delta_\epsilon = -3.5 \cdot 10^{-2}$. We find it amusing to see that it is the triangle graph that generates these large contributions. [In the self-energy type graph (s_{19}), one has to expand the neutral pion mass in the propagator around the charged pion mass. This expansion generates a triangle-type graph.] A graph with triangle-topology was found to generate a large contribution to the photo production of neutral pions a long time ago [40]. In addition, that contribution is responsible for the breakdown of a so-called low-energy theorem in that process. Further, this graph also plays an important role in the low-energy analysis of pion-nucleon scattering [18,32].

One might worry that the next-to-leading order correction could be large as compared to the leading order, and jeopardize the chiral expansion also in the isospin breaking sector. However, as we already noticed, the reason for this large correction is well understood - it is due to the triangle graphs. We do therefore not consider this to be a problem.

Finally, we display in the table the contributions from the counterterms in $\delta\mathcal{T}^{\text{ct}}$, using the estimates displayed above. It is seen that the effect of the LECs at this order is indeed suppressed with respect to the leading order ones. We then add the central values at the scale $\mu = M_\rho$, with $f_1 = g_i^r = k_i^r = 0$. For the uncertainty, we add in quadrature the contributions from f_1 , δf_2 , δc_1 , $k_1^r + k_2^r$, $g_6^r + g_8^r$ and from δd_5^r . In this manner, we obtain

$$\delta_\epsilon = (-7.2 \pm 2.9) \cdot 10^{-2} . \quad (11.3)$$

This is our final result for the correction δ_ϵ . The uncertainty in (11.3) is dominated by the largely unknown coupling f_1 , as is seen from the third row in table 1. It does not take into account contributions from order p^4 in the chiral expansion of the isospin breaking amplitude $\delta\mathcal{T}$.

We note that our numerical results for the isospin-breaking corrections in the amplitude cannot be directly confronted with those of Ref. [17], which refer to different physical quantities. Numerical values for the isospin-breaking effects given in Ref. [17] are typically of order $\sim 1 - 2 \%$.

11.2 Comparison with model calculations

Here we compare our result with the potential model calculation performed in Ref. [6], and with the evaluation [39] of the couplings at leading order in a quark model, Eq. (10.7). We start with the latter. The central values in (10.7) lead⁷ - adding the bound state correction K - to $\delta_\epsilon = -2 \cdot 10^{-2}$ at order p^2 . Taken at face value, this determines the coupling f_1 in our calculation: $f_1 = -1.43 \text{ GeV}^{-1}$, in agreement with the estimate (10.6). This leads finally to $\delta_\epsilon = -4.3 \cdot 10^{-2}$ at order p^3 .

⁷ In Ref. [39] slightly different values for the pion masses were used. The result quoted there for the correction to the energy shift corresponds to those values. We thank V. Lyubovitskij for correspondence.

We now come to the potential model discussed in Ref. [6], which predicts

$$\delta_\epsilon = (-2.1 \pm 0.5) \cdot 10^{-2} . \quad (11.4)$$

We have the following comments.

- The result (11.4) looks considerably more precise than the effective field theory evaluation. There are no unknown LECs occurring in the framework used in Ref. [6].
- The leading terms in the effective field theory framework - that lead to the large uncertainty in (11.3) - are on the other hand not all incorporated [13] in (11.4). An example of a QCD diagram, whose contribution is completely omitted, is shown in Fig. 8. In the potential model [6], it can emerge neither from the $n\gamma$ channel (there is no intermediate state with a neutron in Fig. 8), nor from the Coulomb rescattering (the photon in Fig. 8 is attached only to the proton). At the level of the effective Lagrangians, such contributions are encoded in the low-energy constants f_1 and f_2 .
- The potential model used in Ref. [6] takes into account terms at order p^3 , p^4 , \dots in the language of the low-energy expansion. We are not aware of a proof that it includes all of them. On the other hand, one can construct potentials that certainly do [12]. Unfortunately, these potentials do not determine the LECs, because the LECs are used instead to pin down the potentials.
- The observation that potential models do not, in general, include all effects of QCD+QED is not new. Aside from the hadronic atom case [8,9,10,11], we mention here the investigation of Fettes and Meißner in πN scattering [17]. These authors pointed out that graphs like the one displayed in Fig. 9 (v_6) generate a very large effect, that has not been fully accounted for in existing phase shift analyses.
- We conclude that the uncertainty in (11.4) is underestimated - it does not reflect the systematic errors inherent in the method.

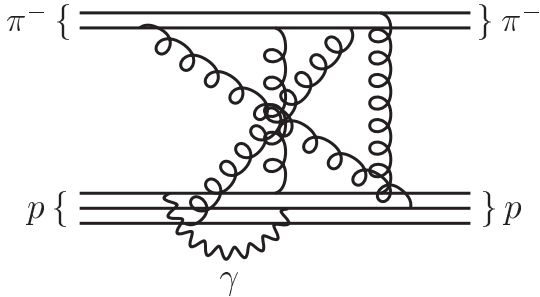


Fig. 8. An example of a QCD diagram, which is not taken into account in the potential model of Ref. [6]. Wiggly lines denote gluons.

12 Summary and conclusions

1. The aim of the present work was to evaluate the ground-state energy of pionic hydrogen in the framework of QCD+QED. We have performed the calculation at next-to-leading order in the low-energy expansion, relying on the method of effective field theories. According to the investigations of Ref. [13], all that is needed for this purpose is an evaluation of the elastic πN scattering amplitude at order p^3 .
2. In order to achieve this goal, we have invoked relativistic baryon ChPT in manifestly Lorentz invariant form [18], and generalized the procedure to allow for virtual photons. To have a powerful check on our calculation, we have in addition performed a heat-kernel evaluation of the ultraviolet divergences at order p^3 , using a consistent set of low-energy meson-meson and meson-nucleon effective Lagrangians that are used in the calculation of the πN scattering amplitudes at $O(p^3)$.
3. We have then calculated the $\pi^- p$ elastic scattering amplitude at threshold - in the presence of isospin breaking - at $O(p^3)$ in the low-energy expansion. The result contains unitarity corrections and counterterm contributions generated by LECs. The quark mass difference $m_d - m_u$ only enters at order p^4 , which is not considered here.
4. At leading order, the contribution to the energy shift is generated [13] by three counterterms f_1 , f_2 and c_1 . Whereas the latter two can be determined from other sources, the size of f_1 needs yet to be determined in a model-independent manner.
5. The loop contributions, which contain mass splitting effects from diagrams with strong loops, turn out to be sizeable. Graphs with a particular topology (triangle graphs) turn out to be particularly important - their contribution to the energy shift indeed is large and negative, a sizeable fraction of the leading order term. Graphs with the same topology play an important role e.g. in photo production of neutral pions [40].
6. The LECs at next-to-leading order are suppressed by one power of M_π and thus expected to have a small effect on the energy shift. This expectation turns out to be correct for one of the couplings that has recently been determined [32] in a comprehensive analysis of πN scattering. Estimating the size of the remaining terms with dimensional arguments, it indeed turns out that their contribution is about an order of magnitude smaller than the leading order result. The final result is given in Eq. (11.3)
7. Whereas it is true that we cannot yet provide a reliable error estimate of the final result, because f_1 is not known with sufficient accuracy, it is also true that the calculation is systematic: The result (9.3)-(9.5) for the threshold amplitude allows one to evaluate the energy-level shift (at this order in the low-energy expansion) from first principles, once one has worked out a reliable estimate for the LECs.
8. A precise determination of the scattering lengths $a_{0+}^+ + a_{0+}^-$ from a precise measurement of the ground-state energy-level shift of pionic hydrogen has to await a

more precise determination of f_1 in our opinion. This fact is hidden in the potential model calculation [6], that quotes a very small uncertainty. As we outlined above, this result does not reflect all systematic uncertainties hidden in this approach: potentials in general do not incorporate the constraints from QCD+QED, unless one imposes these constraints on them [12]. A method different from effective field theories to perform this matching is not in sight. We conclude that one is bound to know the LECs, quite independently of the framework used.

We thank T. Becher, G. Colangelo, G. Ecker, T. Ericson, B. Kubis, H. Leutwyler, V.E. Lyubovitskij, H. Neufeld, U.-G. Meißner, and M.E. Sainio for interesting discussions, and G. Ecker, U.-G. Meißner and H. Neufeld for useful comments on the manuscript. The work was fulfilled while M.A.I., E.L. and M.M. visited the University of Bern. This work was supported in part by the Swiss National Science Foundation, and by TMR, BBW-Contract No. 97.0131 and EC-Contract No. ERBFMRX - CT980169 (EURODAΦNE), and by SCOPES Project No. 7UZPJ65677. M.A.I. appreciates the partial support by the Russian Fund of Basic Research under Grant No. 01-02-17200.

A Meson–meson and meson–nucleon Lagrangians

In this appendix, we give the operator basis and the divergent parts of the LECs of the meson–meson and meson–nucleon effective chiral Lagrangians, that were used in the calculations. We set the charge matrices to their physical, constant values,

$$\mathcal{Q} = \frac{e}{3} \text{diag}(2, -1) \ , \quad Q = e \text{diag}(1, 0) \ , \quad (\text{A1})$$

and use the following notation,

$$\begin{aligned} [D_\mu, X] &\doteq \partial_\mu X + [\Gamma_\mu, X] \ , \\ \bar{\Psi} (O + \text{h.c.}) \Psi &\doteq \bar{\Psi} O \Psi + \text{h.c.} \ , \\ \bar{\Psi} i(O - \text{h.c.}) \Psi &\doteq i(\bar{\Psi} O \Psi - \text{h.c.}) \ , \end{aligned} \quad (\text{A2})$$

where X denotes any bosonic operator, and Ψ is a fermionic field. We use the notation of Bjorken-Drell [21] for the Dirac matrices.

Table 2. Operator basis and the divergent parts of the low-energy couplings in the $O(p^4)$ meson Lagrangian [23] and in the $O(e^2 p^2)$ meson Lagrangian [24]. The terms that do not contain pion fields, and terms of order e^4 are not displayed.

i	$O_i^{(p^4)}$	γ_i
1	$\frac{1}{4} \langle d^\mu U^\dagger d_\mu U \rangle^2$	$\frac{1}{3}$
2	$\frac{1}{4} \langle d^\mu U^\dagger d^\nu U \rangle \langle d_\mu U^\dagger d_\nu U \rangle$	$\frac{2}{3}$
3	$\frac{1}{16} \langle \chi^\dagger U + U^\dagger \chi \rangle^2$	$-\frac{1}{2}$
4	$\frac{1}{4} \langle d^\mu U^\dagger d_\mu \chi + d^\mu \chi^\dagger d_\mu U \rangle$	2
5	$\langle \mathcal{R}^{\mu\nu} U \mathcal{L}_{\mu\nu} U^\dagger \rangle$	$-\frac{1}{6}$
6	$\frac{i}{2} \langle \mathcal{R}^{\mu\nu} d_\mu U d_\nu U^\dagger + \mathcal{L}^{\mu\nu} d_\mu U^\dagger d_\nu U \rangle$	$-\frac{1}{3}$
7	$-\frac{1}{16} \langle \chi^\dagger U - U^\dagger \chi \rangle^2$	0
i	$O_i^{(e^2 p^2)}$	σ_i
1	$\langle d^\mu U^\dagger d_\mu U \rangle \langle \mathcal{Q}^2 \rangle$	$-\frac{27}{20} - \frac{1}{5} Z$
2	$\langle d^\mu U^\dagger d_\mu U \rangle \langle \mathcal{Q} U \mathcal{Q} U^\dagger \rangle$	$2Z$
3	$\langle d^\mu U^\dagger \mathcal{Q} U \rangle \langle d_\mu U^\dagger \mathcal{Q} U \rangle + \langle d^\mu U \mathcal{Q} U^\dagger \rangle \langle d_\mu U \mathcal{Q} U^\dagger \rangle$	$-\frac{3}{4}$
4	$\langle d^\mu U^\dagger \mathcal{Q} U \rangle \langle d_\mu U \mathcal{Q} U^\dagger \rangle$	$2Z$
5	$\langle \chi^\dagger U + U^\dagger \chi \rangle \langle \mathcal{Q}^2 \rangle$	$-\frac{1}{4} - \frac{1}{5} Z$
6	$\langle \chi^\dagger U + U^\dagger \chi \rangle \langle \mathcal{Q} U \mathcal{Q} U^\dagger \rangle$	$\frac{1}{4} + 2Z$
7	$\langle (\chi U^\dagger + U \chi^\dagger) \mathcal{Q} + (\chi^\dagger U + U^\dagger \chi) \mathcal{Q} \rangle \langle \mathcal{Q} \rangle$	0
8	$\langle (\chi U^\dagger - U \chi^\dagger) \mathcal{Q} U \mathcal{Q} U^\dagger + (\chi^\dagger U - U^\dagger \chi) \mathcal{Q} U^\dagger \mathcal{Q} U \rangle$	$\frac{1}{8} - Z$
9	$\langle d_\mu U^\dagger [\mathcal{C}_R^\mu, \mathcal{Q}] U + d_\mu U [\mathcal{C}_L^\mu, \mathcal{Q}] U^\dagger \rangle$	$\frac{1}{4}$
10	$\langle \mathcal{C}_R^\mu U \mathcal{C}_{L\mu} U^\dagger \rangle$	0

Table 3. Operator basis in the $O(p^2)$ pion-nucleon Lagrangian [25], and in the $O(e^2)$ pion-nucleon Lagrangian [27].

i	$O_i^{(p^2)}$	$O_i^{(e^2)}$
1	$\langle \chi_+ \rangle$	$\langle \hat{Q}_+^2 - Q_-^2 \rangle$
2	$-\frac{1}{4m^2} \langle u_\mu u_\nu \rangle (D^\mu D^\nu + \text{h.c.})$	$\langle Q_+ \rangle \hat{Q}_+$
3	$\frac{1}{2} \langle u_\mu u^\mu \rangle$	$\langle \hat{Q}_+^2 + Q_-^2 \rangle$
4	$\frac{i}{4} \sigma^{\mu\nu} [u_\mu, u_\nu]$	
5	$\hat{\chi}_+$	
6	$\frac{1}{8m} \sigma^{\mu\nu} F_{\mu\nu}^+$	
7	$\frac{1}{8m} \sigma^{\mu\nu} \langle F_{\mu\nu}^+ \rangle$	

Table 4. Operator basis and the divergent parts of the low-energy couplings in the third-order strong pion-nucleon Lagrangian. The operator basis is the same as the one used in Ref. [25] for the relativistic operators. The divergent parts are different from Ref. [25], since we use the EOM to eliminate additional operators that arise in the HBChPT formulation, and work with a different basis in the mesonic sector. For comparison with Ref. [26], see appendix B.

i	$O_i^{(p^3)}$	β_i
1	$-\frac{1}{2m} ([u_\mu, [D_\nu, u^\mu]] D^\nu + \text{h.c.})$	$-\frac{1}{6} g_A^4$
2	$-\frac{1}{2m} ([u_\mu, [D^\mu, u_\nu]] D^\nu + \text{h.c.})$	$-\frac{1}{12} - \frac{5}{12} g_A^2$
3	$\frac{1}{12m^3} ([u_\mu, [D_\nu, u_\lambda]] \times (D^\mu D^\nu D^\lambda + \text{sym}) + \text{h.c.})$	$\frac{1}{2} + \frac{1}{6} g_A^4$
4	$-\frac{1}{2m} (\varepsilon^{\mu\nu\alpha\beta} \langle u_\mu u_\nu u_\alpha \rangle D_\beta + \text{h.c.})$	0
5	$\frac{i}{2m} ([\chi_-, u_\mu] D^\mu - \text{h.c.})$	$-\frac{5}{24} + \frac{5}{24} g_A^2$
6	$\frac{i}{2m} ([D^\mu, \hat{F}_{\mu\nu}^+] D^\nu - \text{h.c.})$	$-\frac{1}{6} - \frac{5}{6} g_A^2$
7	$\frac{i}{2m} ([D^\mu, \langle F_{\mu\nu}^+ \rangle] D^\nu - \text{h.c.})$	0
8	$\frac{i}{2m} (\varepsilon^{\mu\nu\alpha\beta} \langle \hat{F}_{\mu\nu}^+ u_\alpha \rangle D_\beta - \text{h.c.})$	0
9	$\frac{i}{2m} (\varepsilon^{\mu\nu\alpha\beta} \langle F_{\mu\nu}^+ \rangle u_\alpha D_\beta - \text{h.c.})$	0
10	$\frac{1}{2} \gamma^\mu \gamma_5 u_\mu \langle u^\nu u_\nu \rangle$	$\frac{1}{2} g_A + \frac{5}{2} g_A^3$
11	$\frac{1}{2} \gamma^\mu \gamma_5 u^\nu \langle u_\mu u_\nu \rangle$	$\frac{1}{2} g_A - \frac{3}{2} g_A^3$
12	$-\frac{1}{8m^2} (\gamma^\mu \gamma_5 u_\mu \langle u_\nu u_\lambda \rangle \times \{D^\nu, D^\lambda\} + \text{h.c.})$	$-2g_A - g_A^3$
13	$-\frac{1}{8m^2} (\gamma^\mu \gamma_5 u_\lambda \langle u_\mu u_\nu \rangle \times \{D^\nu, D^\lambda\} + \text{h.c.})$	$g_A^3 + \frac{2}{3} g_A^5$
14	$\frac{i}{4m} (\sigma^{\mu\nu} \langle u_\nu [D_\lambda, u_\mu] \rangle D^\lambda - \text{h.c.})$	$\frac{1}{3} g_A^4$
15	$\frac{i}{4m} (\sigma^{\mu\nu} \langle u_\mu [D_\nu, u_\lambda] \rangle D^\lambda - \text{h.c.})$	0
16	$\frac{1}{2} \gamma^\mu \gamma_5 \langle \chi_+ \rangle u_\mu$	$\frac{1}{2} g_A + g_A^3$
17	$\frac{1}{2} \gamma^\mu \gamma_5 \langle \chi_+ u_\mu \rangle$	0
18	$\frac{i}{2} \gamma^\mu \gamma_5 [D_\mu, \chi_-]$	g_A
19	$\frac{i}{2} \gamma^\mu \gamma_5 [D_\mu, \langle \chi_- \rangle]$	$-\frac{1}{2} g_A$
20	$-\frac{i}{8m^2} (\gamma^\mu \gamma_5 [\hat{F}_{\mu\nu}^+, u_\lambda] \times \{D^\nu, D^\lambda\} - \text{h.c.})$	$g_A + g_A^3$
21	$\frac{i}{2} \gamma^\mu \gamma_5 [\hat{F}_{\mu\nu}^+, u^\nu]$	$-g_A^3$
22	$\frac{1}{2} \gamma^\mu \gamma_5 [D^\nu, F_{\mu\nu}^-]$	0
23	$\frac{1}{2} \varepsilon^{\mu\nu\alpha\beta} \gamma_\mu \gamma_5 \langle u_\nu F_{\alpha\beta}^- \rangle$	0

Table 5. Operator basis and the divergent parts of the low-energy couplings in the third-order electromagnetic pion-nucleon Lagrangian. The operator basis is the same as the one used in Ref. [28] for the relativistic operators (modulo signs and factors of i), whereas the divergent parts are different from those displayed in Ref. [28], see appendix B.

i	$O_i^{(e^2 p)}$	η_i
1	$\frac{1}{2} \langle Q_+^2 - Q_-^2 \rangle \gamma^\mu \gamma_5 u_\mu$	$g_A(2 + g_A^2 + 4Z + 12g_A^2 Z)$
2	$\frac{1}{2} \langle Q_+ \rangle^2 \gamma^\mu \gamma_5 u_\mu$	$-\frac{1}{2} g_A(3 + 2g_A^2 + 4Z + 12g_A^2 Z)$
3	$\frac{1}{2} \gamma^\mu \gamma_5 \langle Q_+ \rangle \langle Q_+ u_\mu \rangle$	$\frac{1}{2} g_A(1 - 4Z + 4g_A^2 Z)$
4	$\frac{1}{2} \gamma^\mu \gamma_5 Q_+ \langle Q_+ u_\mu \rangle$	$g_A(-1 + 4Z - 4g_A^2 Z)$
5	$\frac{1}{2} \gamma^\mu \gamma_5 Q_- \langle Q_- u_\mu \rangle$	$g_A(3 - 2g_A^2 - 4Z + 4g_A^2 Z)$
6	$\frac{i}{2m} \langle Q_+ \rangle \langle Q_- u_\mu \rangle D^\mu + \text{h.c.}$	$\frac{3}{4} - 3g_A^2$
7	$\frac{i}{2m} Q_- \langle Q_+ u_\mu \rangle D^\mu + \text{h.c.}$	$-\frac{9}{2} - \frac{2}{3} Z$
8	$\frac{i}{2m} Q_+ \langle Q_- u_\mu \rangle D^\mu + \text{h.c.}$	$-\frac{10}{3} g_A^2 Z$
9	$-\frac{1}{2m} [Q_+, c_\mu^+] D^\mu + \text{h.c.}$	$-\frac{3}{2} + 6g_A^2$
10	$-\frac{1}{2m} [Q_-, c_\mu^-] D^\mu + \text{h.c.}$	$+\frac{2}{3} Z + \frac{10}{3} g_A^2 Z$
11	$\frac{i}{2} \gamma^\mu \gamma_5 [Q_+, c_\mu^-]$	-2
12	$\frac{i}{2} \gamma^\mu \gamma_5 [Q_-, c_\mu^+]$	$-\frac{1}{2} + \frac{9}{2} g_A^2$
		$-g_A$
		g_A

B Divergent counterterms

It is common and useful in ChPT to identify the divergent parts of counterterms not just within a calculation of a particular process, but rather in full generality, using the background field and heat-kernel methods. One of the benefits of such an approach is that it provides a nontrivial check for any particular calculation - the loop infinities must be cancelled by the a priori known counterterms.

In spite of the fact that the method of Ball [41] can accommodate large variety of regularizations, including the dimensional one, it is not straightforward to extend it to cover also the Becher-Leutwyler infrared regularization [18,32]. One may, however, utilize the fact that divergences encountered in the infrared regularization are the same as those occurring in heavy baryon ChPT [18,32].

In HBChPT the baryon field is split into velocity-dependent "heavy" and "light" components⁸

$$\begin{aligned} N_v(x) &= e^{imv \cdot x} P_v^+ \Psi(x), \\ H_v(x) &= e^{imv \cdot x} P_v^- \Psi(x), \\ P_v^\pm &= \frac{1}{2} (1 \pm \gamma^\mu v_\mu) \quad ; \quad v^2 = 1, \end{aligned} \quad (\text{B1})$$

and the heavy component $H_v(x)$ is integrated out. The propagator of the remaining light component is a homogeneous function of the residual momentum $k_\mu = p_\mu - mv_\mu$, leading to a consistent chiral power counting in dimensionally regularized HBChPT.

The heat-kernel method in HBChPT leads to a lengthy and cumbersome calculation. The amount of work required can be reduced significantly by introduction of the so-called super-heat-kernel method in recent work of Neufeld *et al* [29,30]. Following closely the procedure of Neufeld, we worked out the complete divergence structure of the one-loop generating functional corresponding to the Lagrangian

$$\mathcal{L} = \mathcal{L}_{HB}^{(p)} + \mathcal{L}_\pi^{(p^2)} + \mathcal{L}_\pi^{(e^2)} + \mathcal{L}_\gamma, \quad (\text{B2})$$

where

$$\mathcal{L}_{HB}^{(p)} = \bar{N}_v (i v^\mu D_\mu + g_A S^\mu u_\mu) N_v \quad (\text{B3})$$

is the HB projection of $\mathcal{L}_N^{(p)}$, with $S^\mu = \frac{i}{2} \gamma_5 \sigma^{\mu\nu} v_\nu$.

The starting point of the background field machinery is a decomposition of fields in the Lagrangian into background fields and fluctuations. Here one has to distinguish between two different elements of the chiral coset space $SU(2)_L \times SU(2)_R / SU(2)_V$, namely u_L and u_R , occurring in the definitions of various fields appearing in chiral invariant Lagrangians,

$$\begin{aligned} U &= u_R u_L^\dagger, \\ u_\mu &= i \left[u_R^\dagger (\partial_\mu - i R_\mu) u_R - u_L^\dagger (\partial_\mu - i L_\mu) u_L \right], \\ \Gamma_\mu &= \frac{1}{2} \left[u_R^\dagger (\partial_\mu - i R_\mu) u_R + u_L^\dagger (\partial_\mu - i L_\mu) u_L \right]. \end{aligned} \quad (\text{B4})$$

Decomposing the fields into classical background fields and fluctuations

$$\begin{aligned} u_R &= u_{cl} e^{i\boldsymbol{\xi}/2F}, & u_L &= u_{cl}^\dagger e^{-i\boldsymbol{\xi}/2F}, \\ N &= N_{cl} + \eta, & A^\mu &= A_{cl}^\mu + \epsilon^\mu, \end{aligned} \quad (\text{B5})$$

and switching to the Euclidean formulation of the theory, which is more convenient when dealing with photons, one first merges the bosonic fields into 7- component objects $\tilde{\xi}$,

$$\tilde{\xi}^T = (\xi^1, \xi^2, \xi^3, \epsilon^0, \epsilon^1, \epsilon^2, \epsilon^3), \quad \boldsymbol{\xi} = \sum \xi^i \boldsymbol{\tau}^i. \quad (\text{B6})$$

⁸ We follow the tradition of denoting the velocity by the same symbol v_μ which was used for the external vector field. The meaning should be always clear from the context.

At the next step, one expands the action up to second order in the fluctuations $\tilde{\xi}$ and η (Euclidean analog of the formula (3.1) in Ref. [30]). Once the explicit form of the fluctuations is worked out, one can use (the Euclidean version of) Neufeld's master equations (3.19)-(3.21), Ref. [30]. At the end, the results are transformed back to Minkowski space.

After some straightforward, yet tedious, algebra one finds the divergent counterterm Lagrangian in a "raw" form,

$$\mathcal{L}^{\text{raw}} = \mathcal{L}_\pi^{\text{raw}} + \mathcal{L}_{\pi\gamma}^{\text{raw}} + \mathcal{L}_N^{\text{raw}} + \mathcal{L}_{N\gamma}^{\text{raw}}, \quad (\text{B7})$$

$$\begin{aligned} \mathcal{L}_\pi^{\text{raw}} &= \frac{1}{16\pi^2(d-4)} \left\{ \frac{1}{12} \langle u \cdot u \rangle^2 + \frac{1}{6} \langle u_\mu u_\nu \rangle \langle u^\mu u^\nu \rangle \right. \\ &\quad + \frac{3}{32} \langle \chi_+ \rangle^2 - \frac{1}{12} \langle \hat{\mathcal{F}}_{+\mu\nu} \hat{\mathcal{F}}_+^{\mu\nu} \rangle \\ &\quad \left. - \frac{i}{12} \langle [u_\mu, u_\nu] \hat{\mathcal{F}}_+^{\mu\nu} \rangle + \frac{1}{4} \langle u \cdot u \rangle \langle \chi_+ \rangle \right\}, \end{aligned} \quad (\text{B8})$$

$$\begin{aligned} \mathcal{L}_{\pi\gamma}^{\text{raw}} &= \frac{F^2}{16\pi^2(d-4)} \left\{ -\frac{27+4Z}{20} \langle u \cdot u \rangle \langle \mathcal{Q}^2 \rangle \right. \\ &\quad + 2Z \langle u \cdot u \rangle \langle \mathcal{Q}_+^2 - \mathcal{Q}_-^2 \rangle \\ &\quad + \frac{3}{2} \left(\langle u_\mu \mathcal{Q}_+ \rangle^2 + \langle u_\mu \mathcal{Q}_- \rangle^2 \right) \\ &\quad + 2Z \left(\langle u_\mu \mathcal{Q}_+ \rangle^2 - \langle u_\mu \mathcal{Q}_- \rangle^2 \right) \\ &\quad - \frac{5+4Z}{20} \langle \chi_+ \rangle \langle \mathcal{Q}^2 \rangle + \frac{1+8Z}{4} \langle \chi_+ \rangle \langle \mathcal{Q}_+^2 - \mathcal{Q}_-^2 \rangle \\ &\quad - \frac{i}{2} \langle u_\mu [\mathcal{C}_-^\mu, \mathcal{Q}_+] + u_\mu [\mathcal{C}_+^\mu, \mathcal{Q}_-] \rangle \\ &\quad + \frac{75-80Z+168Z^2}{50} F^2 \langle \mathcal{Q}^2 \rangle^2 \\ &\quad - \frac{15+2Z+12Z^2}{5} F^2 \langle \mathcal{Q}_+^2 - \mathcal{Q}_-^2 \rangle \langle \mathcal{Q}^2 \rangle \\ &\quad + \frac{3+4Z+24Z^2}{2} F^2 \langle \mathcal{Q}_+^2 - \mathcal{Q}_-^2 \rangle^2 \\ &\quad \left. + \frac{i}{2} \langle [D_\mu, u^\mu] [\mathcal{Q}_-, \mathcal{Q}_+] \rangle \right\}, \end{aligned} \quad (\text{B9})$$

$$\begin{aligned} \mathcal{L}_N^{\text{raw}} &= \frac{1}{16\pi^2(d-4)} \frac{1}{F^2} \bar{N} \left\{ \frac{g_A^4}{8} [u_\mu, [iv \cdot D, u^\mu]] \right. \\ &\quad - \frac{1+5g_A^2}{12} [u_\mu, [iD^\mu, v \cdot u]] \\ &\quad + \frac{4-g_A^4}{8} [v \cdot u, [iv \cdot D, v \cdot u]] \\ &\quad \left. + \frac{4g_A - g_A^5}{8} S \cdot u \langle u \cdot u \rangle \right\} \end{aligned}$$

$$\begin{aligned}
& + \frac{6g_A - 6g_A^3 + g_A^5}{12} u_\mu \langle u^\mu S \cdot u \rangle \\
& + \frac{-8g_A + g_A^5}{8} S \cdot u \langle (v \cdot u)^2 \rangle \\
& - \frac{g_A^5}{12} v \cdot u \langle v \cdot u S \cdot u \rangle + \frac{4g_A - g_A^3}{8} S \cdot u \langle \chi_+ \rangle \\
& - \frac{1 + 5g_A^2}{6} [D_\mu, \hat{F}_+^{\mu\nu}] v_\nu + g_A i S_\mu v_\nu [\hat{F}_+^{\mu\nu}, v \cdot u] \\
& - \frac{4g_A^3 + 3g_A^5}{16} i v_\lambda \varepsilon^{\lambda\mu\nu\rho} \langle u_\mu u_\nu u_\rho \rangle \\
& - \frac{g_A^4}{4} [S^\mu, S^\nu] \langle u_\mu [iv \cdot D, u_\nu] \rangle \\
& - \frac{1 + 5g_A^2}{12} [[iD_\mu, u^\mu], v \cdot u] \\
& - \frac{g_A^3}{4} v_\lambda \varepsilon^{\lambda\mu\nu\rho} \langle \hat{F}_{+\mu\nu} u_\rho \rangle - 3g_A^2 i (v \cdot D)^3 \\
& + g_A^3 v \cdot \overleftarrow{D} S \cdot uv \cdot \overrightarrow{D} \\
& - \frac{12g_A^2 + 9g_A^4}{16} (\langle u \cdot u \rangle iv \cdot D + \text{h.c.}) \\
& + \frac{8 + 9g_A^4}{16} (\langle (v \cdot u)^2 \rangle iv \cdot D + \text{h.c.}) \\
& + \frac{g_A^3}{3} ([v \cdot D, S \cdot u] v \cdot D + \text{h.c.}) \\
& - \frac{9g_A^2}{16} (\langle \chi_+ \rangle iv \cdot D + \text{h.c.}) \\
& + \frac{4g_A^2 + g_A^4}{4} ([S^\mu, S^\nu] u_\mu u_\nu iv \cdot D + \text{h.c.}) \\
& + g_A^2 ([S^\mu, S^\nu] \hat{F}_{+\mu\nu} v \cdot D + \text{h.c.}) \Big\} N, \tag{B10}
\end{aligned}$$

$$\begin{aligned}
\mathcal{L}_{N\gamma}^{\text{raw}} = & \frac{1}{16\pi^2(d-4)} \bar{N} \left\{ \frac{g_A}{2} (8Z - g_A^2) \langle Q_+^2 - Q_-^2 \rangle S \cdot u \right. \\
& - \frac{g_A}{2} (4 + 4Z - g_A^2) \langle Q_+ \rangle^2 S \cdot u \\
& - 2g_A (1 + Z - Zg_A^2) \langle Q_+ S \cdot u \rangle \langle Q_+ \rangle \\
& + 4Zg_A (1 - g_A^2) \langle Q_+ S \cdot u \rangle Q_+ \\
& + 2g_A (1 - g_A^2) (1 - 2Z) \langle Q_- S \cdot u \rangle Q_- \\
& + (1 - 3g_A^2) \langle Q_- v \cdot u \rangle \langle Q_+ \rangle - 4 \langle Q_+ v \cdot u \rangle Q_- \\
& - 2 (1 - 3g_A^2) \langle Q_- v \cdot u \rangle Q_+ - 2 [Q_+, iv \cdot c_+] \\
& - \frac{1}{2} (1 - 9g_A^2) [Q_-, iv \cdot c_-] \\
& \left. - 2 (\langle Q_+ \rangle Q_+ + iv \cdot D + \text{h.c.}) \right\}
\end{aligned}$$

$$\begin{aligned}
& - \frac{1}{4} (2 + 3g_A^2 + 24Zg_A^2) (\langle Q_+^2 - Q_-^2 \rangle iv \cdot D + \text{h.c.}) \\
& + \frac{1}{4} (2 + 3g_A^2 + 12Zg_A^2) (\langle Q_+ \rangle^2 iv \cdot D + \text{h.c.}) \Big\} N. \tag{B11}
\end{aligned}$$

The results for $\mathcal{L}_\pi^{\text{raw}}$ and $\mathcal{L}_{\pi\gamma}^{\text{raw}}$ are consistent with Eq. (A.11) of Ref. [24]⁹, and the result for $\mathcal{L}_N^{\text{raw}}$ is consistent with that of Ref. [42] (to be precise, our $\mathcal{L}_N^{\text{raw}}$ is equal to the final result of Ref. [42], up to the replacement $[D_\mu, u^\mu] \rightarrow \frac{i}{2}\chi_- - \frac{i}{4}\langle\chi_-\rangle$). The result for $\mathcal{L}_{N\gamma}^{\text{raw}}$ agrees with Steininger's expression [28], Eq. (3.124) up to several signs and factors of i [Note e.g. that the expression (3.124) in Ref. [28] is not hermitean, according to the definition (2.9) in that work.].

The "raw" divergent Lagrangian, obtained so far, can be consistently used for renormalization of any process up to the corresponding order. On the other hand, it is perhaps not the most convenient choice, since it differs from the standard Lagrangians used in the field. To bring our result to the standard form, one has to perform the standard procedure, namely use the basis from Ref. [23] for $\mathcal{L}_\pi^{(p^4)}$, and eliminate some of the terms by using equations of motion (EOM) for the classical fields.

The EOM are obtained from the linear part of the fluctuation Lagrangian,

$$\begin{aligned}
[D_\mu, u^\mu] = & \frac{i}{2}\chi_- - \frac{i}{4}\langle\chi_-\rangle + 4iZF^2[\mathcal{Q}_+, \mathcal{Q}_-] \\
& + \frac{i}{4F^2}\tau^a \bar{N} [\tau^a, v \cdot u] N - \\
& - \left(\frac{g_A}{F^2} \tau^a \bar{N} \tau^a S \cdot DN + \text{h.c.} \right), \\
iv \cdot DN = & -g_A S \cdot u N. \tag{B12}
\end{aligned}$$

Here, we have not included an external source for the nucleon field, because we are only interested in the S -matrix elements. The proper way of using these EOM is to use appropriate field transformations. For the mesonic Lagrangian, however, the use of the lowest order EOM, i.e. replacing the structure $[D_\mu, u^\mu]$ by the RHS of the EOM, is equivalent to the systematic performance of field redefinitions [43]. For the baryonic Lagrangian, the required nucleon field transformations are explicitly given in [26].

The resulting divergent nucleon Lagrangian corresponds exactly to the heavy baryon projections of the Lagrangians (3.3) and the pertinent tables in the appendix A. For the relativistic Lagrangians at $O(p^2)$, $O(p^3)$, $O(e^2p)$, the simple replacements $\gamma_\mu \gamma_5 \rightarrow 2S_\mu$, $iD_\mu \Psi \rightarrow mv_\mu N_v$ and $\sigma_{\mu\nu} \rightarrow -2i[S_\mu, S_\nu]$ are all what is needed. Note that in appendix A we do not display terms in the Lagrangians $\mathcal{L}_\pi^{(p^4)}$ and $\mathcal{L}_\pi^{(e^2p^2)}$, which do not contain pion fields. In addition, we drop all terms at $O(e^4)$.

We wish to note that all β -functions given in the table 2, coincide with the ones from Refs. [23,24]. The β -

⁹ There are misprints in that equation, not present in the final result displayed in Eq. (3.6) of that work.

functions from table 4 are consistent with the results of Ref. [26] (the latter contains a misprint in β_{11} , $2/3g_A^5 \rightarrow -2/3g_A^5$). Note that in Ref. [26], a different basis in the mesonic sector was used - consequently, in order to compare, one has to transform the β -functions, see below. After this is done, β_i from table 4 are equal to β_i ($i = 1 \dots 3$) and to β_{i+1} ($i = 4 \dots 23$) of table 1, Ref. [26]. The entries of the table 5, necessary for a coherent result, were, to best of our knowledge, not presented yet. As it has been mentioned above, the β -functions for the $O(e^2 p)$ Lagrangian, which were presented in Ref. [28], and were used in the numerical fits in Ref. [17], correspond to the “raw” form (B11), rather than to the Lagrangian which is brought to the “standard” form in the mesonic sector by using the EOM.

Finally, we comment on the relation between the two most commonly used choices of operator basis in the $\mathcal{L}_\pi^{(p^4)}$ Lagrangian. Some of the β -functions are changed when one changes the basis from [23] to [31] (the barred quantities belong to the latter basis)

$$\begin{aligned}\bar{\beta}_5 &= \frac{1+5g_A^2}{24}, & \bar{\beta}_{18} &= 0, \\ \bar{\beta}_{19} &= 0, & \bar{\sigma}_8 &= \frac{1}{8}.\end{aligned}\quad (\text{B13})$$

Furthermore, some of the renormalized LECs do differ in the two bases, namely

$$\begin{aligned}\bar{d}_5^r(\mu) &= d_5^r(\mu) + \frac{1}{8F^2} l_4^r(\mu), \\ \bar{d}_{18} &= d_{18}^r(\mu) - \frac{g_A}{2F^2} l_4^r(\mu), \\ \bar{d}_{19} &= d_{19}^r(\mu) + \frac{g_A}{4F^2} l_4^r(\mu), \\ \bar{k}_8^r(\mu) &= k_8^r(\mu) + \frac{1}{2} Z l_4^r(\mu).\end{aligned}\quad (\text{B14})$$

C Integrals

In this appendix, we present some useful formulae that we have used in the calculations. Note that all formulae given here correspond to the case of standard dimensional regularization.

In the diagrams with virtual photons, the following definite integrals over the Feynman parameter x are needed [here, $R = x + (1-x)r^2 - x(1-x)\bar{s}$ is a quadratic polynomial in x , and $\bar{s} \doteq s/m^2 \geq (1+r)^2$],

$$\begin{aligned}\int_0^1 dx \ln R &= -2 + x_- \ln \frac{x_-}{1-x_-} + x_+ \ln \frac{x_+}{1-x_+} - i\pi\sigma_0 \\ &= -2 + \frac{2r \ln r}{1+r} - i\pi\sigma_0 + O(\sigma_0),\end{aligned}\quad (\text{C1})$$

$$\begin{aligned}\int_0^1 dx \frac{1}{R} &= \frac{1}{\bar{s}\sigma_0} \left\{ \ln \frac{x_-}{1-x_-} - \ln \frac{x_+}{1-x_+} + 2i\pi \right\} \\ &= -\frac{1}{r} + i\pi \frac{2}{(1+r)^2\sigma_0} + O(\sigma_0),\end{aligned}\quad (\text{C2})$$

$$\begin{aligned}\int_0^1 dx \frac{x}{R} &= \frac{1}{\bar{s}\sigma_0} \left\{ x_- \ln \frac{x_-}{1-x_-} \right. \\ &\quad \left. - x_+ \ln \frac{x_+}{1-x_+} + i\pi(x_- + x_+) \right\} \\ &= -\frac{1+r+\ln r}{(1+r)^2} + i\pi \frac{2r}{(1+r)^3\sigma_0} + O(\sigma_0),\end{aligned}\quad (\text{C3})$$

$$\begin{aligned}\int_0^1 dx \frac{\ln R}{R} &= \frac{1}{\bar{s}\sigma_0} \left\{ 2\text{Li}_2\left(\frac{1-x_+}{1-x_-}\right) + 2\text{Li}_2\left(\frac{x_-}{x_+}\right) \right. \\ &\quad \left. + \frac{4\pi^2}{3} + \frac{1}{2}\ln^2\left(\frac{1-x_+}{1-x_-}\right) + \frac{1}{2}\ln^2\left(\frac{x_-}{x_+}\right) \right. \\ &\quad \left. + 2(\ln \bar{s} + 2\ln \sigma_0) \cdot \left[\frac{1}{2}\ln\left(\frac{1-x_+}{1-x_-}\right) \right. \right. \\ &\quad \left. \left. + \frac{1}{2}\ln\left(\frac{x_-}{x_+}\right) + i\pi \right] \right\} \\ &= \frac{\pi^2}{(1+r)^2} \cdot \frac{2}{\sigma_0} - \frac{2}{r} - \frac{2\ln r}{r(1+r)} \\ &\quad + i\pi \frac{4\ln[(1+r)\sigma_0]}{(1+r)^2\sigma_0} + O(\sigma_0 \ln \sigma_0),\end{aligned}\quad (\text{C4})$$

where

$$\begin{aligned}x_{\pm} &= \frac{\bar{s} - 1 + r^2 \pm \lambda^{1/2}(\bar{s}, 1, r^2)}{2\bar{s}}, \\ \sigma_0 &= x_+ - x_- = \frac{\lambda^{1/2}(\bar{s}, 1, r^2)}{\bar{s}} = \frac{2|\mathbf{p}|}{\sqrt{\bar{s}}}, \\ \lambda(x, y, z) &= (x - y - z)^2 - 4yz, \\ \text{Li}_2(z) &= -\int_0^z dt \frac{\ln(1-t)}{t}.\end{aligned}\quad (\text{C5})$$

We also recall a useful representation [44] of the vertex functions that occur in the diagrams of Fig. 11 (s_{12}), (s_{13}). These are UV and IR finite, so one may put $d = 4$ from the beginning.

$$\begin{aligned}(I_3; I_{3v}^\mu) &= \frac{1}{\pi^2 i} \int d^4 k \frac{(1; k^\mu)}{[m_1^2 - k^2]} \\ &\quad \times \frac{1}{[m_2^2 - (k + p_1)^2][m_3^2 - (k + p_1 + p_2)^2]},\end{aligned}\quad (\text{C6})$$

$$I_{3v}^\mu = I_{31} p_1^\mu + I_{32} p_2^\mu ,$$

$$I_3 = \int_0^1 dx \left\{ \frac{1}{A_1} \ln R_1 - \frac{(1-\alpha_0)}{A_2} \ln R_2 - \frac{\alpha_0}{A_3} \ln R_3 \right\} , \quad (C7)$$

$$I_{31} = \int_0^1 dx \left\{ \frac{1}{A_1} \left[\left(x - 1 - \alpha_0 \frac{R_1}{A_1} \right) \ln R_1 + \alpha_0 \right] - \frac{(1-\alpha_0)}{A_2} \left[\left(x - 1 - \alpha_0 \frac{R_2}{A_2} \right) \ln R_2 + \alpha_0 x \right] - \frac{\alpha_0}{A_3} \left[\left(-1 - \alpha_0 \frac{R_3}{A_3} \right) \ln R_3 + \alpha_0 x \right] \right\} , \quad (C8)$$

$$I_{32} = \int_0^1 dx \left\{ \frac{1}{A_1} \left[\left(-\frac{R_1}{A_1} \right) \ln R_1 + 1 \right] - \frac{(1-\alpha_0)}{A_2} \left[\left(x - 1 - \frac{R_2}{A_2} \right) \ln R_2 + x \right] - \frac{\alpha_0}{A_3} \left[\left(x - 1 - \frac{R_3}{A_3} \right) \ln R_3 + x \right] \right\} , \quad (C9)$$

$$\begin{aligned} R_1 &= x m_1^2 + (1-x) m_2^2 - x(1-x) p_1^2 , \\ R_2 &= x m_1^2 + (1-x) m_3^2 - x(1-x) p_3^2 , \\ R_3 &= x m_2^2 + (1-x) m_3^2 - x(1-x) p_2^2 , \\ p_3^2 &= (p_1 + p_2)^2 , \end{aligned} \quad (C10)$$

$$\begin{aligned} A_1 &= \lambda^{1/2} (p_1^2, p_2^2, p_3^2) \cdot x + a_1 , \\ A_2 &= (1-\alpha_0) \lambda^{1/2} (p_1^2, p_2^2, p_3^2) \cdot x + a_2 , \\ A_3 &= -\alpha_0 \lambda^{1/2} (p_1^2, p_2^2, p_3^2) \cdot x + a_3 , \end{aligned} \quad (C11)$$

$$\begin{aligned} a_1 &= m_2^2 - m_3^2 + p_2^2 + \alpha_0 (m_1^2 - m_2^2 - p_1^2) , \\ a_2 &= a_3 = m_2^2 - m_3^2 - p_2^2 \\ &\quad + \alpha_0 (m_1^2 - m_2^2 + p_2^2 - p_3^2) , \\ \alpha_0 &= \frac{p_1^2 + p_2^2 - p_3^2 + \lambda^{1/2} (p_1^2, p_2^2, p_3^2)}{2 p_1^2} . \end{aligned} \quad (C12)$$

The integrals I_3 , I_{31} and I_{32} are not changed under scaling of the arguments of the logarithms by any arbitrary constant value. This property allows one to replace $\ln R_i \rightarrow \ln R_i/m^2$ in the above expressions. Note that in the threshold amplitude we have $\lambda(p_1^2, p_2^2, p_3^2) = 0$. This considerably simplifies the calculations.

D Contributions from individual Feynman diagrams

In this appendix, we list the non-vanishing contributions to the threshold amplitude, due to the diagrams displayed in Figs. 9,10 and 11. The notation used is the one in (9.1), (9.2). The quantities $C_{UV,IR}$ are defined in Eq. (6.4), and $r = M_\pi/m$.

Table 6. Vector-type electromagnetic diagrams I_V^i in the infrared regularization, up to and including $O(r)$.

Fig. 9	I_V^i
(v_1)	$-\frac{r}{8} (7 C_{UV} + 8 C_{IR} + 16 + 30 \ln r)$
(v_2)	$\frac{r}{8} (7 C_{UV} + 8 C_{IR} + 16 + 30 \ln r)$
(v_3)	$\frac{r}{2} (C_{UV} - C_{IR})$
(v_4)	$-\frac{r}{4} (C_{UV} + 2 C_{IR} - 4 + 6 \ln r)$
(v_5)	0
(v_6)	$-\frac{r}{4} (-3 C_{UV} + 4 - 6 \ln r)$

Table 7. Axial-type electromagnetic diagrams I_A^i in the infrared regularization, up to and including $O(r)$.

Fig. 10	I_A^i
(a_4)	$-6r C_{UV} + 2r - 12r (\ln 2 + \ln r)$
(a_8)	$-3r C_{UV} - 2r - 3r (\pi + 2 \ln r)$
(a_9)	$3r C_{UV} - 2r + 2r (\pi + 2 \ln 2 + 3 \ln r)$

Table 8. Isospin-conserving strong contributions I_0^i and isospin-breaking strong contributions I_π^i in the infrared regularization, up to and including $O(r^3)$ and $O(r)$, respectively.

Fig. 11	I_0^i	I_π^i
(s_{12})	$\frac{g_A^2}{128} r^3 (3 C_{UV} + 2 + 6 \ln r)$	$-\frac{g_A^2}{128} r (3 C_{UV} + 5 + 6 \ln r)$
(s_{13})	$-\frac{g_A^2}{64} r^3 (3 C_{UV} + 2 + 6 \ln r)$	0
(s_{14})	$\frac{1}{32} r^3 (C_{UV} + 2 \ln r)$	0
(s_{15})	$\frac{1}{128} r^3 (-5 C_{UV} + 8 - 10 \ln r)$	$-\frac{1}{128} r (3 C_{UV} + 11 + 6 \ln r)$
(s_{16})	$\frac{1}{256} r^3 (-5 C_{UV} + 8 - 10 \ln r)$	0
(s_{18})	$-\frac{g_A^2}{48} \pi r^3$	0
(s_{19})	$-\frac{g_A^2}{48} \pi r^3$	$\frac{g_A^2}{32} \pi r$
(s_{20})	$-\frac{1}{256} r^3 (-5 C_{UV} + 8 - 10 \ln r)$	0
(s_{21})	$\frac{g_A^2}{96} r^3 (9 C_{UV} + 6 + 2 \pi + 18 \ln r)$	$-\frac{3 g_A^2}{16} \pi r$
(s_{22})	$\frac{13 g_A^2}{192} \pi r^3$	$-\frac{13 g_A^2}{128} \pi r$
(s_{23})	$-\frac{5}{384} r^3 (C_{UV} + 2 \ln r)$	$\frac{1}{384} r (C_{UV} + 1 + 2 \ln r)$

References

1. H.N. Brown *et al.* [Muon g-2 Collaboration], Phys. Rev. Lett. **86**, (2001) 2227 [arXiv:hep-ex/0102017].
2. B. Adeva *et al.*, CERN proposal CERN/SPSLC 95-1 (1995).
3. G.C. Oades *et al.*, *Measurement of the strong interaction width and shift of the ground state of pionic hydrogen*, PSI Proposal R-98-01.
4. H.C. Schroder *et al.*, Eur. Phys. J. **C 21**, (2001) 473.
5. G. Colangelo, J. Gasser and H. Leutwyler, Phys. Lett. **B 488**, (2000) 261 [arXiv:hep-ph/0007112]; Nucl. Phys. **B 603**, (2001) 125 [arXiv:hep-ph/0103088].
6. D. Sigg, A. Badertscher, P.F.A. Goudsmit, H.J. Leisi, and G.C. Oades, Nucl. Phys. **A 609** (1996) 310.
7. A. Gashi, E. Matsinos, G.C. Oades, G. Rasche, and W.S. Woolcock, arXiv:hep-ph/0009081; G. Rasche and W.S. Woolcock, Nucl. Phys. **A 381**, (1982) 405 .
8. V.E. Lyubovitskij and A.G. Rusetsky, Phys. Lett. **B 389**, (1996) 181 [arXiv:hep-ph/9610217]; V.E. Lyubovitskij, E.Z. Lipartia, and A.G. Rusetsky, JETP Lett. **66**, (1997) 783 [arXiv:hep-ph/9801215]; H. Jallouli and H. Sazdjian, Phys. Rev. **D 58**, (1998) 014011 [arXiv:hep-ph/9706450]; P. Labelle and K. Buckley, arXiv:hep-ph/9804201; M.A. Ivanov, V.E. Lyubovitskij, E.Z. Lipartia, and A.G. Rusetsky, Phys. Rev. **D 58**, (1998) 094024 [arXiv:hep-ph/9805356]; X. Kong and F. Ravndal, Phys. Rev. **D 59**, (1999) 014031; Phys. Rev. **D 61**, (2000) 077506 [arXiv:hep-ph/9905539]; B.R. Holstein, Phys. Rev. **D 60**, (1999) 114030 [arXiv:nucl-th/9901041]; D. Eiras and J. Soto, Phys. Rev. **D 61**, (2000) 114027 [arXiv:hep-ph/9905543]; Phys. Lett. **B 491**, (2000) 101 [arXiv:hep-ph/0005066]; H. Sazdjian, Phys. Lett. **B 490**, (2000) 203 [arXiv:hep-ph/0004226].
9. A. Gall, J. Gasser, V.E. Lyubovitskij, and A. Rusetsky, Phys. Lett. **B 462**, (1999) 335 [arXiv:hep-ph/9905309].
10. J. Gasser, V.E. Lyubovitskij, and A. Rusetsky, Phys. Lett. **B 471**, (1999) 244 [arXiv:hep-ph/9910438].
11. J. Gasser, V.E. Lyubovitskij, A. Rusetsky, and A. Gall, Phys. Rev. **D 64**, (2001) 016008 [arXiv:hep-ph/0103157].
12. E. Lipartia, V.E. Lyubovitskij, and A. Rusetsky, Phys. Lett. **B 533**, (2002) 285 [arXiv:hep-ph/0110186].
13. V.E. Lyubovitskij and A. Rusetsky, Phys. Lett. **B 494**, (2000) 9 [arXiv:hep-ph/0009206].
14. G. Höhler, in Landolt-Börnstein, vol. **9 b2**, ed. H. Schopper (Springer, Berlin, 1983).
15. J. Gasser, H. Leutwyler and M.E. Sainio, Phys. Lett. **B 253**, (1991) 252 .
16. M. L. Goldberger, H. Miyazawa and R. Oehme, Phys. Rev. **99**, (1955) 986 .
17. N. Fettes and U.-G. Meißner, Nucl. Phys. **A 693**, (2001) 693 [arXiv:hep-ph/0101030].
18. T. Becher and H. Leutwyler, Eur. Phys. J. **C 9**, (1999) 643 [arXiv:hep-ph/9901384].
19. U.-G. Meißner and S. Steininger, Phys. Lett. **B 419**, (1998) 403 [arXiv:hep-ph/9709453].
20. D. Eiras and J. Soto, Phys. Lett. **B 491**, (2000) 101 [arXiv:hep-ph/0005066].
21. J.D. Bjorken and S.D. Drell, Relativistic Quantum Fields, McGraw-Hill, Inc., 1965.
22. D.R. Yennie, S.C. Frautschi, and H. Suura, Ann. Phys. **13**, (1961) 379.
23. J. Gasser and H. Leutwyler, Annals Phys. **158**, (1984) 142.

24. M. Knecht and R. Urech, Nucl. Phys. **B 519**, (1998) 329 [arXiv:hep-ph/9709348].
25. N. Fettes, U.-G. Meißner and S. Steininger, Nucl. Phys. **A 640**, (1998) 199 [arXiv:hep-ph/9803266].
26. G. Ecker and M. Mojzis, Phys. Lett. **B 365**, (1996) 312 [arXiv:hep-ph/9508204].
27. G. Müller and U.-G. Meißner, Nucl. Phys. **B 556**, (1999) 265 [arXiv:hep-ph/9903375].
28. S. Steininger, “*Reelle und virtuelle Photonen in chiraler Störungstheorie*”, Ph.D. thesis, University of Bonn (1999).
29. H. Neufeld, J. Gasser and G. Ecker, Phys. Lett. **B 438**, (1998) 106 [arXiv:hep-ph/9806436].
30. H. Neufeld, Eur. Phys. J. **C 7**, (1999) 355 [arXiv:hep-ph/9807425].
31. J. Gasser, M.E. Sainio and A. Svarc, Nucl. Phys. **B 307**, (1988) 779.
32. T. Becher and H. Leutwyler, JHEP **0106**, (2001) 017 [arXiv:hep-ph/0103263].
33. N. Fettes and U. G. Meißner, Nucl. Phys. **A 676**, (2000) 311 [arXiv:hep-ph/0002162].
34. R. Koch, Nucl. Phys. **A 448**, (1986) 707.
35. D.E. Groom *et al.* [Particle Data Group Collaboration], Eur. Phys. J. **C 15**, (2000) 1.
36. P. Buttiker and U.-G. Meißner, Nucl. Phys. **A 668**, (2000) 97 [arXiv:hep-ph/9908247].
37. J. Gasser and H. Leutwyler, Phys. Rept. **87**, (1982) 77.
38. N. Fettes and U.-G. Meißner, Phys. Rev. **C 63** (2001) 045201 [arXiv:hep-ph/0008181].
39. V.E. Lyubovitskij, Th. Gutsche, A. Faessler, and R. Vinh Mau, Phys. Lett. **B 520**, (2001) 204 [arXiv:hep-ph/0108134]; Phys. Rev. **C 65**, (2002) 025202 [arXiv:hep-ph/0109213].
40. V. Bernard, N. Kaiser, J. Gasser and U.-G. Meißner, Phys. Lett. **B 268**, (1991) 291; V. Bernard, N. Kaiser and U.-G. Meißner, Z. Phys. **C 70**, (1996) 483 [arXiv:hep-ph/9411287].
41. R.D. Ball, Phys. Rep. **182**, (1989) 1.
42. G. Ecker, Phys. Lett. **B 336**, (1994) 508 [arXiv:hep-ph/9402337].
43. J. Bijnens, G. Colangelo and G. Ecker, JHEP **9902**, (1999) 020 [arXiv:hep-ph/9902437].
44. G. t’Hooft and M.J.G. Veltman, Nucl. Phys. **B 153**, (1979) 365.

E Figures

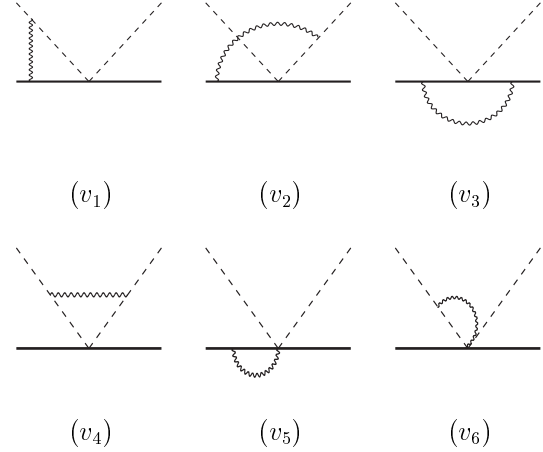
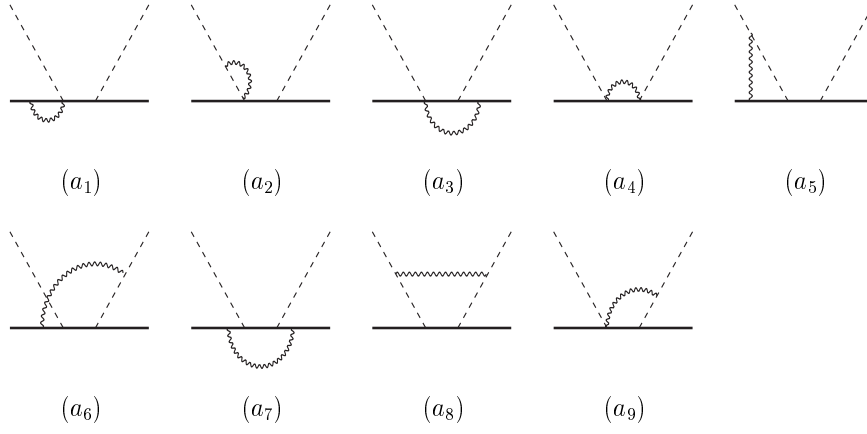
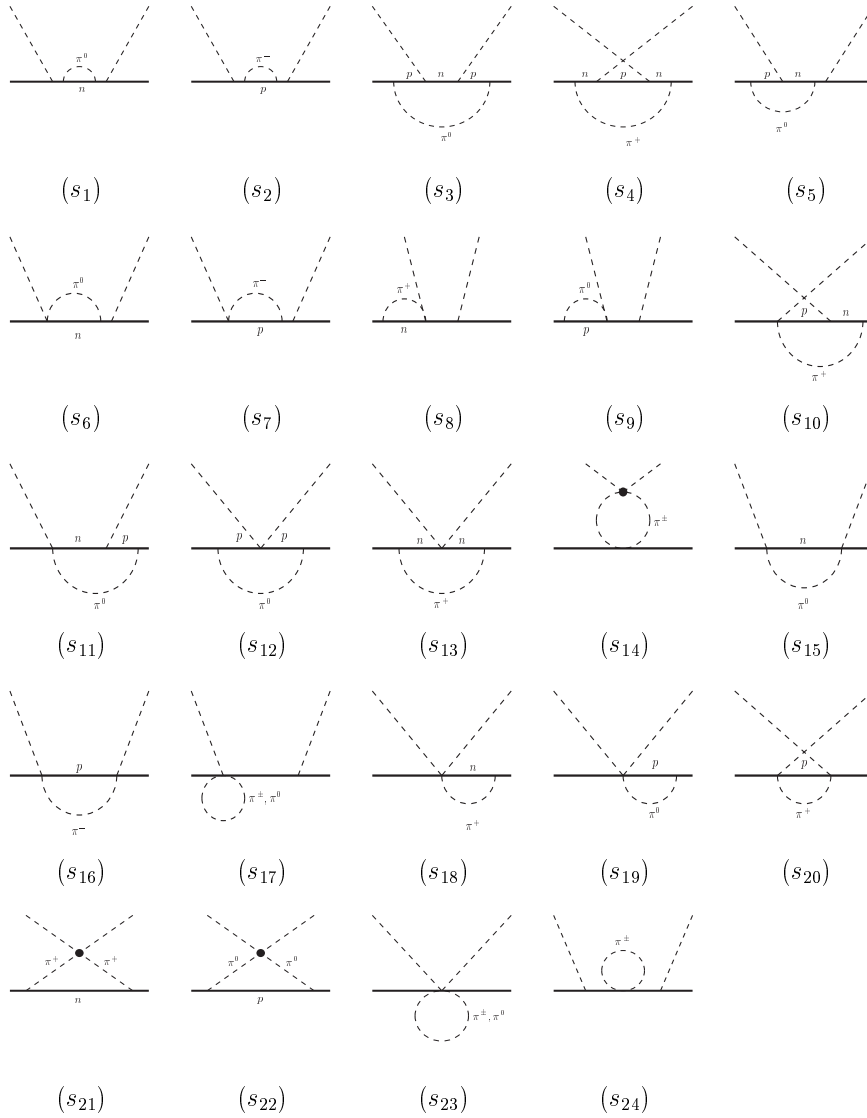


Fig. 9. The electromagnetic vector-type diagrams.

**Fig. 10.** The electromagnetic axial-type diagrams.**Fig. 11.** The strong one-loop diagrams.